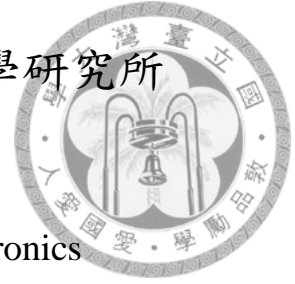國立臺灣大學電機資訊學院光電工程學研究所

博士論文

Graduated Institute of Photonics and Optoelectronics

College of Electrical Engineering and Computer Science

National Taiwan University

Doctoral Thesis

探討金奈米圓盤於氮化鎵奈米柱陣列上之

特高頻音波偵測

Investigation of Gold Nanodisk on GaN Nanorod Arrays

for Hypersonic Detection

楊思齊

Szu-Chi Yang

指導教授：孫啟光 博士

Advisor: Chi-Kuang Sun, Ph.D.

中華民國 一百零四年 七 月

July, 2015

國立臺灣大學博士學位論文
口試委員會審定書

探討金奈米圓盤於氮化鎵奈米柱陣列上之
特高頻音波偵測
Investigation of Gold Nanodisk on GaN Nanorod
Arrays for Hypersonic Detection

本論文係楊思齊君（學號 D00941009）在國立臺灣大學
光電工程學研究所完成之博士學位論文，於民國 104 年 7 月
22 日承下列考試委員審查通過及口試及格，特此證明

口試委員：

孫啟光 （指導教授）

張之威　　　　黃升明

林恬孜　　　　吳政達

所長 林恭如

致謝

摘要

近年來，超音波成像已經被廣泛應用來取得非透明表面下之影像。在成像系統中，單一元件超音波換能器或超音波陣列可利用氧化鋅或壓電陶瓷來產生超音波。理論上，成像系統的解析度會被音波波長所決定，因此高頻的音波可以提供更高的影像解析度。舉例來說，過去曾有團隊利用單一元件超音波換能器來產生 15.3 吉赫的超音波來成像。但是在單一元件的系統中，必須要搭配音波的聚焦鏡來收集音波。相反地，超音波陣列只需要分析每個像素所量測的訊號，即可重建出影像。但目前的超音波陣列所能偵測的頻率仍在次吉赫波段，若是能將超音波陣列所偵測的波段提升到 10 吉赫以上，對未來的特高頻音波成像上可以產生極大的幫助。

在這篇論文中，我們證明了金奈米圓盤於氮化鎵奈米柱陣列上的結構可用來偵測 10 吉赫以上的音波。在此結構中,侷限性表面電漿子可大幅提高偵測靈敏度，並且消除每個奈米圓盤之間的電漿耦合。因此每個金奈米圓盤可以視為獨立的偵測結構。此外，我們也發現金奈米圓盤所偵測的訊號與陣列的週期，以及奈米柱的長度都有關係。當週期小於音波的波長時，所偵測的訊號會受到奈米柱間的震動膜態耦合所影響。這個效應可以藉由改變奈米柱長度，使得奈米柱的震動頻率遠離我們的操作頻率來消除。而當週期小於音波的波長時，表面音波會在奈米柱間產生共振，進而影響音波的穿透率。此研究不僅探討特高頻音波在奈米柱與材料基板間的傳遞,此外也闡明了在未來特高頻音波陣列的設計上所需注意的事項，對未來的高解析特高頻音波成像系統可望做出許多貢獻。

Abstract

Acoustic imaging technique was demonstrated as an efficient method to obtain the structure below the opaque sample surface non-destructively. In traditional ultrasonic imaging, acoustic transducers such as single element transducers or phased array systems are widely utilized. In these setups, acoustic waves are generated by piezoelectric materials, such as ZnO or lead zirconate titanate (PZT). Theoretically the system resolution will be limited by the diffraction of the acoustic waves. In order to achieve high resolution acoustic image, imaging systems intend to utilize high frequency acoustic waves. For example, an acoustic microscope applied the ZnO single element transducer to detect the hypersonic waves with 15.3 GHz in pressurized superfluid helium. However the acoustic lens was always necessary in the system based on a single element transducer. On the contrary, phased array system allows dynamic image reconstruction at different depths below the sample surface, which provides better flexibility and capability in detection setups. However, the highest operation frequency of the phased array systems is in the sub-GHz region. Therefore it is highly desirable to extend the detection frequency of phased arrays to above 10 GHz for high resolution imaging.

In this thesis, we demonstrate that gold nanodisks on GaN nanorod array have a great potential to be utilized as a hypersonic array. The lowest detection frequency is the fundamental confined acoustic vibrations of gold nanodisks, which is around 10 GHz. In this structure, the hypersonic detection sensitivity can be enhanced by optically exciting localized surface plasmons at the gold/GaN interface, which makes each gold nanodisk as an independent opto-acoustic detector through eliminating the plasmonic

IV

coupling between gold nanodisks. For array imaging application, we further apply this structure to passively detect the hypersonic waves and to study the effect of the array periodicity.
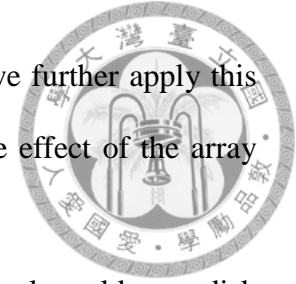
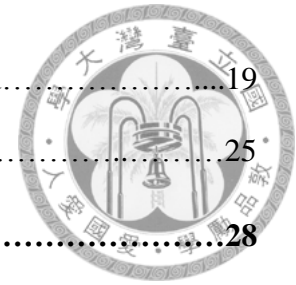Our results show that the hypersonic signal detected by single gold nanodisk depends on the array periodicity. When the periodicity is smaller than the surface hypersonic wavelength, signal detection would be affected by the coupling of the extensional-vibration-like mode of neighboring nanorods as the detection frequency approached such vibrational mode frequency. This coupling effect could be avoided by increasing the nanorod length to shift the frequency of the extensional mode away from the detection frequency. On the contrary, when the periodicity is on the order of or longer than the wavelength of surface hypersonic waves, the detected signal is affected by the period-dependent resonance of surface hypersonic waves scattered from the nanorod/substrate interface. By studying the transport behavior of hypersonic-frequency acoustic phonons at the bulk-material/nano-structure interface, this work not only investigate the possibility of hypersonic array for high resolution acoustic imaging purpose, but also suggests that effects of the periodicity and nanorod length on the individual nanodisk responses need to be taken into consideration for future hypersonic imaging array design.

Contents
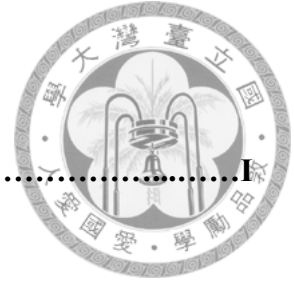
Figure Contents

Chapter 1

Introduction

1.1 Acoustic Imaging Technique

Acoustic imaging is a powerful technique that has been applied in a variety of fields such as medical imaging [1], underwater detection [2] and non-destructive testing [3]. In traditional ultrasonic imaging, acoustic transducers such as single element transducer [4, 5] or phased array system [6, 7] are widely utilized. In these systems, acoustic waves are electronically generated by piezoelectric material, such as ZnO [8] or piezoelectric material lead zirconate titanate (PZT) [9]. In the most of imaging system, the highest resolution of the system will be limited by the diffraction. In order to achieve higher resolution in the acoustic image, imaging system is intend to utilize shorter wavelength (high frequency) acoustic waves. For example, an acoustic microscopy based on the ZnO single element transducer enables the detection of 15.3 GHz hypersonic waves in pressurized superfluid helium [10] (the frequency of hypersonic waves ranges from 1 GHz to 1 THz). However the acoustic lens is always necessary in the system of single element transducer. In contrast to the single element transducer, phased array system allows the image reconstruction at different depths below the sample surface by analyzing the signal received by each transducer in the array. Phased array system thus provides better flexibility and capability in detection setups. However, the highest operation frequency of the phased array systems is in the sub-GHz region [11]. Therefore it is highly desirable to extend the detection frequency of phased array to above 10 GHz for high resolution imaging purpose.

1.2 Femtosecond Time Resolved Spectroscopy

In this thesis, we studied the possibility of hypersonic phased array by focusing on the detection of hypersonic waves in the array system. Hypersonic pulse with nm pulse width was launched to the array and induced the vibration of the acoustic detector. Due to the fact that acoustic pulse consists of a large number of frequency components, we were thus able to analyze the frequency response of our system. In this work, the vibration of our transducer was studied by the femtosecond time resolved spectroscopy. This technique allows the observation with femtosecond time resolution, which provides an effective efficacy to study the transient phenomena such as carrier dynamics [12, 13] and hypersonic waves [14, 15] in semiconductors or metals. Fig. 1.1 shows the schematic of the femtosecond time resolved spectroscopy; there are two femtosecond laser beams in the system. One of them is pump beam, which is used to optically excite the hypersonic pulse of the sample. Basically hypersonic waves can be optically generated from many materials such as metal thin film [16, 17], semiconductor thin film [18-20], p-n junction [21], graphene layer [22], quantum wells [23-26], or quantum dots [27, 28]. When femtosecond laser beam is absorbed by these materials, subsequent effects such as thermal expansion in metal [29], electronic stress in semiconductor [30, 31] or the screening the piezoelectric field in quantum wells [32, 33] are stimulated. These effects modify the lattice constant of the material and thus generate the hypersonic waves.

Another femtosecond laser beam is called probe beam, which detects the vibration of transducer induced by the pump beam. In the system, pump beam is usually modulated by the acoustic-optical modulator (AO modulator), therefore we are able to obtain the pump-induced optical change by collecting probe beam with the same
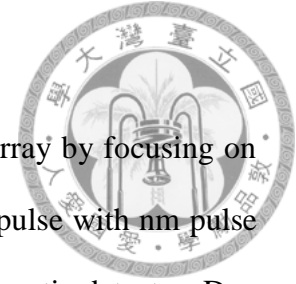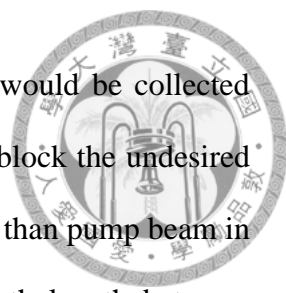
modulation frequency as pump beam. Note that only probe beam would be collected rather than pump beam, an iris is thus placed before the detector to block the undesired pump beam. Theoretically, the power of probe beam is much weaker than pump beam in order to neglect the probe-induced optical change. The optical path length between pump beam and probe beam can be changed by moving the delay stage; probe beam is thus able to detect the pump-induced optical change at different time delay.
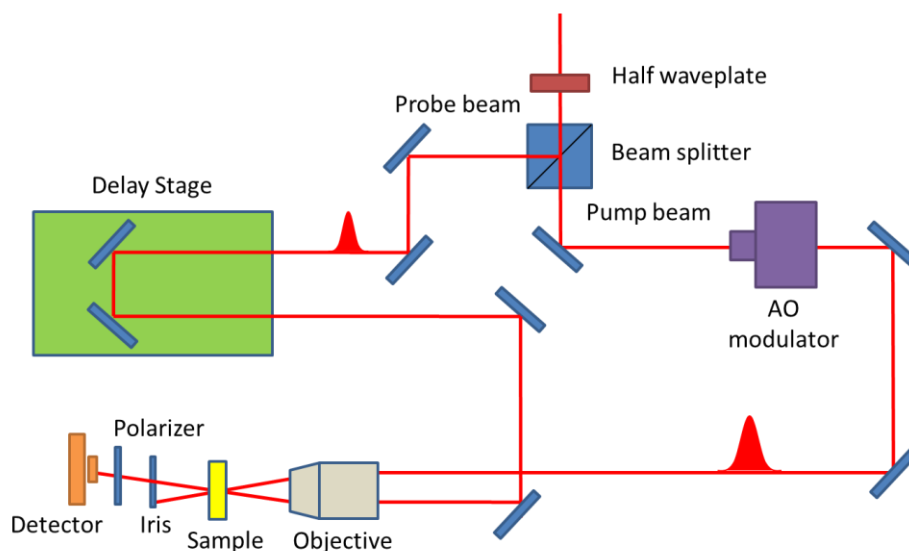
Fig. 1.1 The schematic showing of femtosecond time resolved spectroscopy

1.3 Surface Plasmon Polaritons and Localized Surface Plasmons

In order to enhance the detection sensitivity of the hypersonic array, behaviors of surface plasmon polaritons (SPPs) and localized surface plasmons (LSPs) should also be investigated due to the fact that these plasmonic fields are very sensitive to the environmental disturbance. Basically SPPs and LSPs are collective electron resonance at the interface between metal and dielectric medium. In order to excite SPPs or LSPs, the momentum of the incident light needs to be modified to couple to plasmons. For example, periodic nano-structures such as 1-D metal nanograting [34-36] or 2-D metal

nanodisks array [37, 38] are common structures to excite SPPs. The resonance wavelength of SPPs strongly depends on the incident light angle [39] or the period of the nanostructure [40, 41]. On the other hand, fabrication of the nano-structure is not necessary for the excitation of LSPs [42]. Therefore LSPs are often observed in the metal particle solution [43]. The resonance wavelength of LSPs is not related to the incident light angle [44, 45] but strongly depends on the shape and the size of the particle [46, 47].

Both plasmonic fields of SPPs and LSPs are strongly confined at metal/dielectric interface [48], environmental disturbance at this interface would strongly modify the boundary condition of plasmons. As we mentioned above, such plasmonic field is therefore very sensitive to the environmental disturbance. Based on this characteristic, SPPs and LSPs are widely applied to chemical sensors [49] and biological sensors [50]. Due to the environmental sensitive characteristic of SPPs and LSPs, they are thus good candidates to enhance the detection of hypersonic waves [51-56].

1.4 Thesis Structure

On the basics of the previous discussion, the main purpose of this work is to investigate the possibility of hypersonic array. In order to enhance the detection sensitivity, behaviors of SPPs and LSPs in the system as well as their interaction with the hypersonic pulse are also needed to be studied. Our investigation first started from simple 1-D nanograting structure, and then we extended the structure to 2-D nanodisk array.

In the following chapter, the behaviors of plasmons in the nanostructure (ex. 1-D nanograting and 2-D nanodisks array) are first studied. Then the interaction between

plasmons and hypersonic pulse is investigated to verify the possibility of the proposed hypersonic sensor. Finally the effect of the periodicity of the hypersonic array is discussed. Based on the understanding of these critical issues, hypersonic array system with both high longitudinal and lateral spatial resolution may be realized in the future.
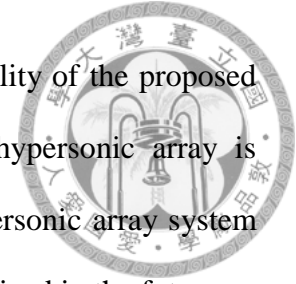
Reference

[1] G. Baum, I. Greenwood, S. Slawski and R. Smirnow, Science **139**, 495−496 (1963).

[2] J. Sutton , Proc. IEEE **67**, 554−566 (1979).

[3] G. Kino , Proc. IEEE **67**, 510−525 (1979).

[4] B. L. Heffner, G. S. Kino and B. T. Khuri-Yakub, Appl. Phys. Lett. **47**, 17 (1985).

[5] B. Hadimioglu and J. S. Foster, Appl. Phys. Lett. **56**, 1976 (1984).

[6] R. Chen, N. E. Cabrera-Munoz, K. H. Lam, H. S. Hsu, F. Zheng, Q. Zhou, K. K. Shung, IEEE Trans. Ultrason. Ferroelectr. Freq. Control **61**, 1033 (2014).

[7] C. Liu, F. T. Djuth, Q. Zhou, K. K.Shung, IEEE Trans. Ultrason. Ferroelectr. Freq. Control **60**, 2615 (2013).

[8] B. Hadimioglu, L. J. La Comb Jr., D. R. Wright, B. T. Khuri-Yakub and C. F. Quate, Appl. Phys. Lett. **50**, 1642 (1987).

[9] A. Jakob, M. Bender, T. Knoll, R. Lemor, M. Bender, T. Lehnert, M. Koch, M. Veith, Q. Zhou, B.P. Zhu, J.X. Han, K.K. Shung, Proc. IEEE Inter. Ultrason. Symp., 1722 (2009).

[10] M. S. Muha, A. A. Moulthrop, G. C. Kozlowski and B. Hadimioglu, Appl. Phys. Lett. **56**, 1019 (1990).

[11] J. Y. Zhang, W. J. Xu, J. Carlier, E. Moulin, D. Remiens, X. M. Ji, Y. P. Huang, S. M. Chen, IEEE Trans. Ultrason. Symp., 1739 (2011).

[12] Y.-E. Su, Y.-C. Wen, Y.-L. Hong, H.-M. Lee, S. Gwo, Y.-T. Lin, L.-W. Tu, H.-L. Liu, and C.-K. Sun, Appl. Phys. Lett. **98**, 252106 (2011).

[13] Y.-E. Su, Y.-C. Wen , H.-M. Lee , S. Gwo, and C.-K. Sun, Appl. Phys. Lett. **96**, 052108 (2010).

[14] P.-A. Mante, Y.-R. Huang, S.-C. Yang, T.-M. Liu, A. Maznev, J.-K. Sheu, C.-K. Sun, Ultrasonics **56**, 52-65 (2015).

[15] A. Maznev, K. J. Manke, K.-H. Lin, K. A. Nelson, C.-K. Sun, and J.-I. Chyi, Ultrasonics **52**, 1-4 (2012).

[16] C. Thomsen, H. T. Grahn, H. J. Maris, and J. Tauc, Phys. Rev. B **34**, 4129–4138 (1986).

[17] H.–N. Lin, R. J. Stoner, H. J. Maris, and J. Tauc, J. Appl. Phys. **69**, 3816–3822 (1991).

[18] O. B. Wright and V. E. Gusev, Appl. Phys. Lett. **66**, 1190–1192 (1995).

[19] S. Wu, P. Geiser, J. Jun, J. Karpinski, and R. Sobolewski, Phys. Rev. B **76**, 085210 (2007).

[20] Y.-H. Chen, Y.-C. Wen, W.-R. Liu, W.-F. Hsieh, and C.-K. Sun, Chin. J. Phys. **49**, 201–208 (2011).

[21] Y.-C. Wen, G.-W. Chern, K.-H. Lin, J. J. Yeh, and C.-K. Sun, Phys. Rev. B **84**, 205315 (2011).

[22] I.-J. Chen, P.-A. Mante, C.-K. Chang, S.-C. Yang, H.-Y. Chen, Y.-R. Huang, L.-C. Chen, K.-H. Chen, V. Gusev, and C.-K. Sun, Nano Lett. **14**, 1317–1323 (2014).

[23] C.-K. Sun, J.-C. Liang, C. J. Stanton, A. Abare, L. Coldren, and S. P. DenBaars, Appl. Phys. Lett. **75**, 1249–1251 (1999).

[24] G.-W. Chern, K.-H. Lin, and C.-K. Sun, J. Appl. Phys. **95**, 1114–1121 (2004).

[25] K.-H. Lin, C.-F. Chang, C.-C. Pan, J.-I. Chyi, S. Keller, U. Mishra, S. P. DenBaars, and C.-K. Sun, Appl. Phys. Lett. **89**, 143103 (2006).

[26] C.-C. Chen, H.-M. Huang, T.-C. Lu, H.-C. Kuo, and C.-K. Sun, Appl. Phys. Lett. **100**, 201905 (2012).

[27] P.-A. Mante, A. Devos, and A. Le Louarn, Phys. Rev. B **81**, 113305 (2010).

[28] Y.-C. Wen, J.-H. Sun, C. Dais, D. Gr€utzmacher, T.-T. Wu, J.-W. Shi, and C.-K. Sun, Appl. Phys. Lett. **96**, 123113 (2010).

[29] C. Thomsen, J. Strait, Z. Vardeny, H. J. Maris, J. Tauc, and J. J. Hauser, Phys. Rev. Lett. **53**, 989 (1984).

[30] A. Bartels, T. Dekorsy, K. Kurz, and K. Kohler, Phys. Rev. Lett. **82**, 1044 (1999).

[31] R. G. Stearns and G. S. Kino, Appl. Phys. Lett. **47**, 1048 (1985).

[32] C. K. Sun, J. C. Liang, and X. Y. Yu, Phys. Rev. Lett. **84**, 179 (2000).

[33] C. K. Sun, Y. K. Huang, J. C. Liang, A. Abare, and S. P. DenBaars, Appl. Phys. Lett. **78**, 1201 (2001).

[34] H. L. Offerhaus, B. van den Bergen, M. Escalante, F. B. Segerink, J. P. Korterik, and N. F. van Hulst, Nano Letters **5**, 2144 (2005).

[35] E. Devaux, T. W. Ebbesen, J. C. Weeber, and A. Dereux, Appl. Phys. Lett. **83**, 4936 (2003).

[36] S. Park, G. Lee, S. H. Song, C. H. Oh, and P. S. Kim, Opt. Lett. **28**, 1870 (2003).

[37] Y. Chu, E. Schonbrun, T. Yang, and K. B. Crozier, Appl. Phys. Lett. **93**, 181108 (2008).

[38] P.J. Rodríguez-Cantó, M. Martínez-Marco, F. J. Rodríguez-Fortuño, B. Tomás-Navarro, R. Ortuño, S. Peransí-Llopis, A. Martínez, Opt. Express **19**, 7664-7672 (2011).

[39] A. O. Pinchuk, J. Phys. Chem. A **113**, 4430–4436 (2009).

[40] L. L. Zhao, K. L. Kelly, and G.C. Schatz, J. Phys. Chem. B **107**, 7343 (2003).

[41] C. L. Haynes, A. D. McFarland, L. L. Zhao, R. P. Van Duyne, G. C. Schatz, L. Gunnarsson, J. Prikulis, B. Kasemo, and M. J. Kall, Phys. Chem. B **107**, 7337 (2003).

[42] P. Hanarp, M. Kall, and D. S. Sutherland, J. Phys. Chem. B **107**, 5768-5772 (2003).

[43] F. Mafuné, J.-Y. Kohno , Y. Takeda , and T. Kondow, J. Phys. Chem. B **104**, 8333–8337 (2000).

[44] C.-M.Wang, Y.-C. Chang, M.-W. Tsai, Y.-H. Ye, C.-Y. Chen, Y.-W. Jiang, Y.-T. Chang, S.-C. Lee, and D.-P. Tsai, Opt. Express **15**, 14673 (2007).

[45] M. N. Abbas, C.-W. Cheng, Y.-C. Chang, M.-H. Shih, H.-H. Chen and S.-C. Lee, Appl. Phys. Lett. **98**, 121116 (2011).

[46] J. P. Kottmann, O. J. F. Martin, D. R. Smith, and S. Schultz, Phys. Rev. B **64**, 235402 (2001).

[47] K. L. Kelly , E. Coronado , L. L. Zhao , and G. C. Schatz, J. Phys. Chem. B **107**, 668–677 (2003).

[48] A. G. Brolo, R. Gordon, B. Leathem, and K. L. Kavanagh, Langmuir **20**, 4813–4815 (2004).

[49] R. Gordon, D. Sinton, K. L. Kavanagh, and A. G. Brolo, Acc. Chem. Res. **41**, 1049–1057 (2008).

[50] K.-L. Lee, S.-H. Wu, and P.-K. Wei, Opt. Express **17**, 23104–23113 (2009).

[51] J. Wang, J. Wu, and C. Guo, Opt. Lett. **32**, 719–721 (2007).

[52] H.-P. Chen, Y.-C. Wen, Y.-H. Chen, C.-H. Tsai, K.-L. Lee, P.-K. Wei, J.-K. Sheu, and C.-K. Sun, Appl. Phys. Lett. **97**, 201102 (2010).

[53] C. Bruggemann, J. Jager, B. A. Glavin, V. I. Belotelov, I. A. Akimov, S. Kasture, A.

V. Gopal, A. S. Vengurlekar, D. R. Yakovlev, A. V. Akimov, and M. Bayer, Appl. Phys. Lett. **101**, 243117 (2012).

[54] S.-C. Yang, H.-P. Chen, H.-H. Hsiao, P.-K. Wei, H.-C. Chang, and C.-K. Sun, Opt. Express **20**, 16186 (2012).

[55] C. Bruggemann, A. V. Akimov, B. A. Glavin, V. I. Belotelov, I. A. Akimov, J. Jager, S. Kasture, A. V. Gopal, A. S. Vengurlekar, D. R. Yakovlev, A. J. Kent, and M. Bayer, Phys. Rev. B. **86**, 121401 (2012).

[56] P.-A. Mante, H.-Y. Chen, M.-H. Lin, Y.-C. Wen, S. Gwo, and C.-K. Sun, Appl. Phys. Lett. **101**, 101903 (2012).

Chapter 2

Plasmonic Excitation for Hypersonic Imaging

2.1 Introduction

Recently SPPs and LSPs have attracted many attentions due to the fact that well-confined plasmonic field is very sensitive to the environmental disturbance [1]. Since hypersonic pulse modulates the refractive index of the studied sample, SPPs and LSPs are thus proposed as an effective hypersonic sensor [2-7]. In this chapter, the plasmonic behavior in metallic nanostructure (1-D gold nanogratings and 2-D gold nanodisks array) is first investigated before applying the plasmonic field to the acoustic detection.

2.2 Excitation of Surface Plasmon Polaritons

SPPs are collective electron resonance at the interface between metal and dielectric medium. The dispersion curve of SPPs excited by the TM wave can be expressed as the following equation [8]:

$$k_x = \frac{\omega}{c} \sqrt{\frac{\varepsilon_{metal}\varepsilon_{dielectric}}{\varepsilon_{metal} + \varepsilon_{dielectric}}} \quad (1)$$

Where k_x is the wave vector of SPPs, ω is the angular frequency of SPPs, c is the light speed, ε are dielectric constant of the material. Fig. 2.1 shows the comparison of the dispersion curve between the ordinary incident light (ω/c) and the SPPs. Due to the fact that the light line of the incident light is not able to intersect with the dispersion curve of SPPs, SPPs thus cannot be excited by the ordinary incident light. However the periodic
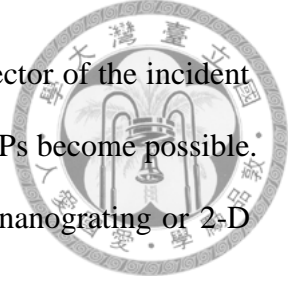
nanostructure could provide extra momentum to modify the wave vector of the incident light, which leads the energy coupling between incident light and SPPs become possible. In the following section, periodic nanostructures such as 1-D gold nanograting or 2-D gold nanodisk array are going to be investigated
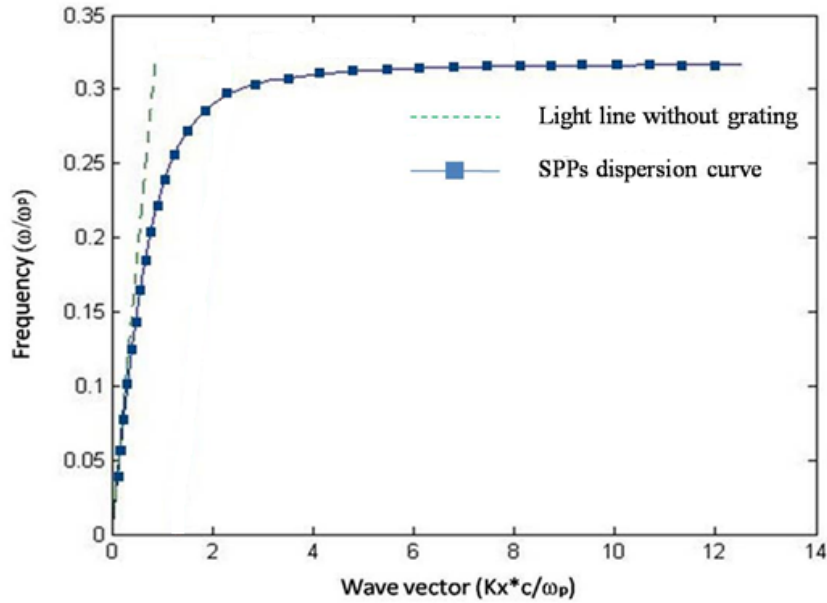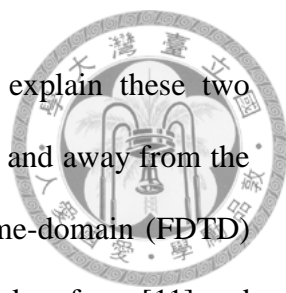
Figure 2.1 The dispersion curves of SPPs and ordinary incident light.

2.2.1 Surface Plasmon Polaritons in 1-D Gold Nanogratings

First we studied the behavior of SPPs in 1-D metallic nanograting. Our studied sample consists of a 1-D gold grating on the plane GaN substrate with a periodicity varying from 590 nm to 650 nm, the heights and the widths of slits are both around 70 nm. Fig. 2.2(a) shows the transmission spectra of the studied sample calculated by rigorous coupled-wave analysis (RCWA) algorithm [9]. We can observe that the wavelength of extraordinary transmission (EOT) shifts as the periodicity of grating increases. Theoretically there are two different types of resonances which are in charge of this behavior. One is SPPs resonance; the other one is cavity mode (CM) resonance. Here

we take the grating with 590 nm periodicity as an example to explain these two resonances. Fig. 2.2(b) shows the optical energy field distribution at and away from the wavelength of EOT, which is calculated by the finite-difference time-domain (FDTD) algorithm [10]. The refractive index values of gold and GaN were taken from [11] and [12], respectively. With an incident wave from the substrate side polarized parallel to the sample surface but perpendicular to nanogratings (x-direction in Fig. 2.2(b)), the E_x field intensity image shows the interaction result between the incident light wave and the scattered light wave. The field pattern below the nanoslit is the result of interference from these two waves. High field intensity can be observed inside the nanoslit and this phenomenon is attributed to the different effective refractive indices between the upper and lower interfaces of the slit, which causes the so-called "cavity mode." [13] Since the incident wave is only x-polarized which propagates along the z-axis, thus the E_z field intensity image reflects the induced electric energy field by the incident wave. For the field distribution at the peak wavelength, the induced E_z field intensity can be found to be well-confined at the gold/GaN interfaces. Since it is well-known that the SPPs field is well confined at the metal/dielectric interface and exponentially decays in the z-direction into the substrate, we thus refer this field as the SPP field [14]. On the other hand, this field is not able to be observed for the wavelength far away from the peak wavelength. Fig. 2.2(c) shows the poynting vector of the simulated energy field distribution at the EOT wavelength. The propagated energy direction of CM resonance and SPPs are vertical and parallel to the sample surface respectively. The energy of SPPs is thus confined well at the gold/GaN interface, only the energy of CM resonance can propagate to the far field. Fig. 2.2(c) also indicates that the energy can transfer from SPPs to CM resonance near the slit edge. Therefore optical energy absorbed by SPPs at

gold/GaN interface is possible to couple to CM resonance, which results in EOT. Consequently, changing the periodicity of the grating would not only modify the behavior of SPPs but also shift the wavelength of EOT.
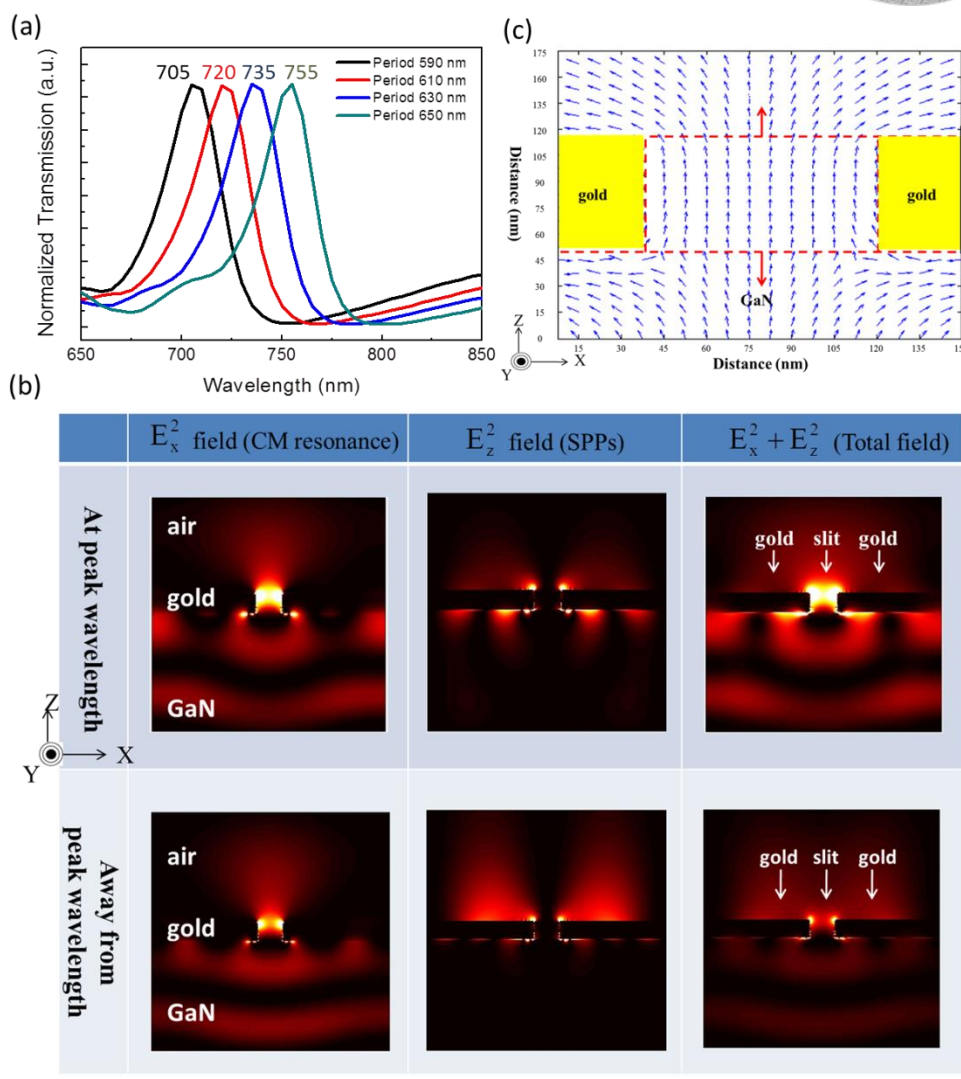
Figure 2.2 (a) The normalized simulated transmission spectra for 1-D gold nanograting on the plain GaN substrate with different periodicities. (b) The simulated energy field distribution of 1-D gold nanograting at and far away from the wavelength of EOT (c) The poynting vector of the energy field at the wavelength of EOT.

Based on the simulation, we fabricated the sample by e-beam lithography. We first grew a 3.7-µm-thick GaN single wurtzite crystal film with 10% thickness fluctuation by Metal-Organic chemical Vapor Deposition (MOCVD) on a double-side polished c-plane sapphire substrate with a 350 µm thickness. A 140-nm-thick E-beam resist layer was coated on the GaN film to define the desired pattern by E-beam lithography. The E-beam resist was Zep520A and the electron dose time was 0.35 µs/dot. After developing the resist by a developer, a 70-nm-thick gold film was then coated on the GaN by thermal evaporation. We finally lifted off the remaining resist and finished the sample processing. The fabricated nanostructure covered an area of 300 µm×300 µm.

Fig. 2.3(a) depicts the example of scanning electron microscopy (SEM) image of 1-D gold nanogratings on a GaN substrate. Periodicity of nanogratings is 590 nm while the height and width of the slit are both 70 nm. Fig. 2.3(b) shows the experimental transmission spectra of the 1-D gold nanograting with different periodicity after normalizing the peak value. The EOT wavelength is red-shift by increasing the periodicity of the grating; furthermore the measured resonant wavelengths of EOT with different grating periodicities show a good agreement with the simulation in Fig. 2.2(a).

(a)

0.5μm

(b)

700 715 730 750

Normalized Transmission (a.u.)

	Period 590nm
	Period 610nm
	Period 630nm
	Period 650nm

650   700   750   800   850

Wavelength (nm)
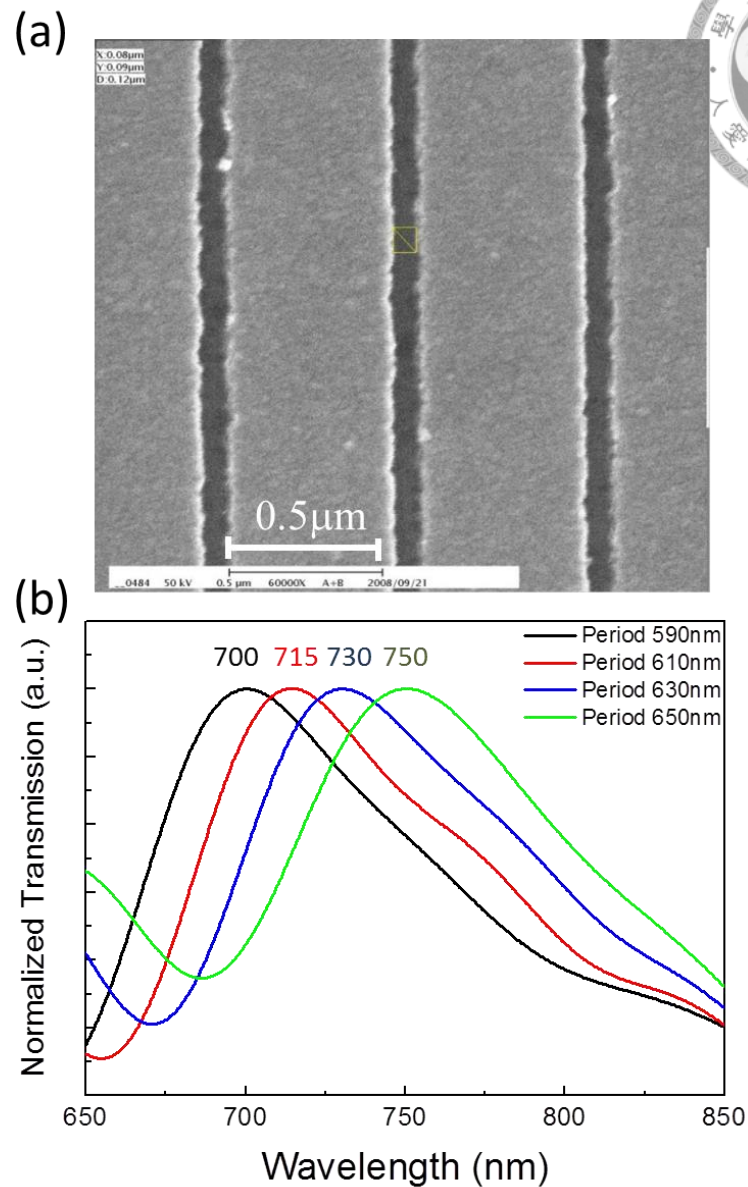
Figure 2.3 (a) The SEM image of 1-D gold nanogratings on a GaN substrate with

590 nm periodicity. (b) The normalized experimental transmission spectra of the 1-D

gold nanograting with different periodicity.

2.2.2 Surface Plasmon Polaritons in 2-D Gold Nanodisks Array

Although SPPs in 1-D gold nanograting may be served as a hypersonic sensor, this

structure however limits the detection only in one dimension. Therefore this is very

important for hypersonic imaging purpose to extend the structure into 2-D metallic

nanodisk array. Our studied sample is gold nanodisks arrays on plain GaN substrate

with 150 nm diameter. The periodicity of the array is varied from 250 nm to 400 nm.

Fig. 2.4(a) shows the simulated extinction spectra of the studied sample, peak

wavelength of the spectrum indicates the resonant wavelength SPPs. It is obvious that

the resonant wavelength of SPPs of nanodisk arrays is red-shift by increasing the

periodicity of the array. This phenomenon is called the dipolar coupling effect [15-17].

When light excite the plasmon resonance in the gold nanodisk, each nanodisk can be

referred as a dipole. The relation between the polarization of the dipole and incident

electric field can be express as the following equation:

$$P = \alpha \cdot E \ (1)$$

Where P and α are the polarization and the polarizability of the dipole, while E is the

incident electric field. For the array structure, these dipoles can couple to each other and

the collective polarizability ($\alpha_{collective}$) should be modified:

$$\alpha_{collective} = \frac{\alpha}{1 - \alpha \cdot S} \ (2)$$

$$S = d^3 \sum_{j \neq i} \left[\frac{(1 - ikr_{ij})(3\cos^2\theta_{ij} - 1)e^{ikr_{ij}}}{r_{ij}^3} + \frac{k^2 \sin^2\theta_{ij} \cdot e^{ikr_{ij}}}{r_{ij}} \right] \ (3)$$

$$C_{ext} = 4\pi k \cdot \text{Im}(\alpha_{collective}) \ (4)$$

r_{ij} is the distance between nanodisks labeled i and j, θ_{ij} is the angle between the

polarization vector and the vector from nanodisk. Therefore changing the period will

modify the coupling strength between nanodisks and affect the collective polarizability.

Due to the fact that the extinction cross-section (C_{ext}) is related to the imaginary part of

the polarizability, the resonant wavelength of SPPs is thus strongly period dependent.
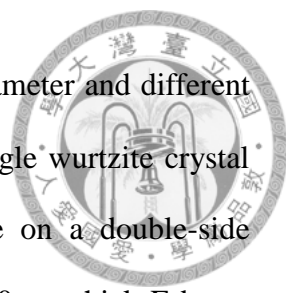
Fig. 2.4(b) shows our fabricated samples with 150 nm disk diameter and different periodicities. In all samples, we first grew a 3.4-μm-thick GaN single wurtzite crystal film with 10% thickness fluctuations by the MOCVD technique on a double-side polished c-plane sapphire substrate with a 350 μm thickness. A 300-nm-thick E-beam resist layer was then spin-coated on the GaN film to define the pattern by E-beam lithography. The E-beam resist was Zep520A and the electron dose time was varied from 0.7~1.1 μs/dot, which depends on the periodicities of the nanodisk arrays. After developing the resist by a developer, a 50-nm-thick gold film was then coated on the GaN sample surface by thermal evaporation. We finally lifted off the remaining resist and finished the sample processing of gold nanodisks on top of plain substrates. Fig. 2.4(c) shows the experimental extinction spectra after normalizing the peak value, the extinction coefficient (σ_{ext}) can be calculated from $I\text{-}I_0 = -\sigma_{ext} NI_0$, where I_0 is the intensity of the incident light, I is the intensity of the transmitted light and N is the density of nanodisks in the pattern [18]. The bandwidth of the measured spectrums are slight broader compared to the simulation due to the size inhomogeneity of the fabricated gold nanodisks. However the resonant wavelengths of SPPs in gold nanodisks arrays with different periodicities still show the good agreement with the simulation.
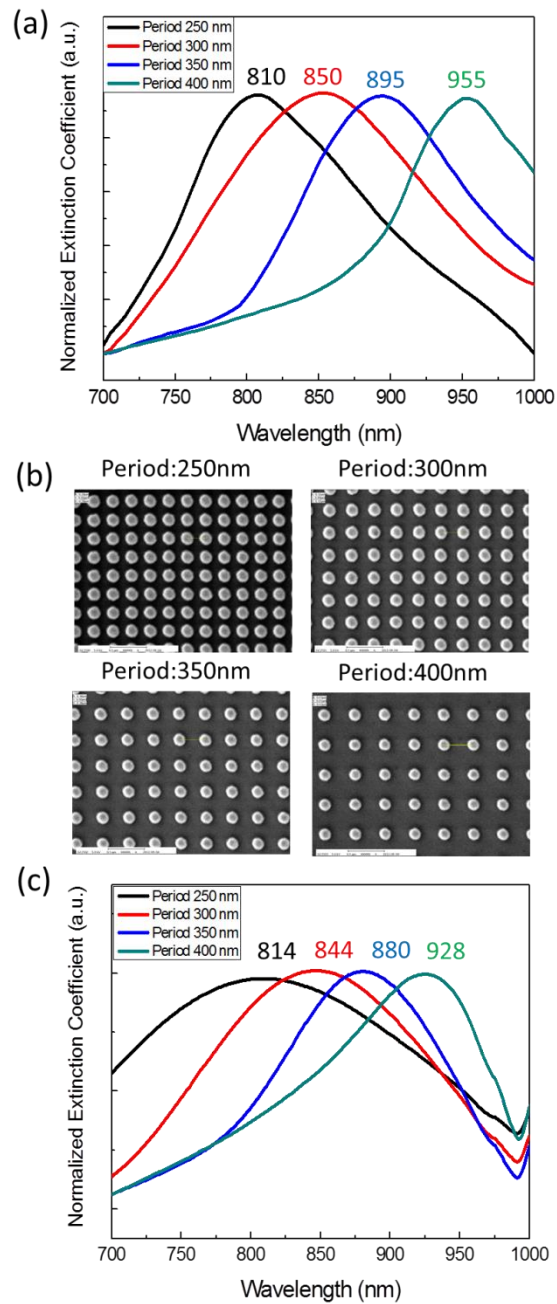
Figure 2.4 (a) The normalized simulated extinction spectra. (b) The SEM images and (c) the normalized experimental extinction spectra of 2-D gold nanodisks arrays with different periodicities.

2.3 Localized Surface Plasmons in 2-D Gold Nanodisks on Nanorod

Although the 2-D gold nanodisks array is able to expand the acoustic detection into another dimension, the dipolar coupling effect among nanodisks would delocalize the plasmonic field intensity and degrade the lateral resolution. Furthermore, the resonant wavelength of SPPs in a 2-D nanodisk array varies with incident light angles. Since most applications of opto-acoustic detection prefer stable and repeatable systems that do not strongly depend on the incident light angle, it is therefore necessary to excite LSPs in a 2-D nanodisk array to eliminate the coupling between neighboring nanodisks and to enhance the angle tolerance of incident light.

Here we propose to modify the plain GaN substrate to nanorod substrate for exciting LSPs [19, 20]. These high-refractive-index nanorods could localize the plasmonic field within the rods, while the air gaps restrict the coupling between gold nanodisks. By suppressing the coupling effect, hypersonic detection using a single nanodisk will not be affected by adjacent nanodisks; i.e., each gold nanodisk can be considered as an independent acoustic sensor. At the same time, the intensity of the plasmonic field can be increased due to the localization of the plasmonic field. This high intensity field can further increase the detection sensitivity [21].

First 2-D gold nanodisk arrays on GaN nanorod arrays are fabricated based on the same sample processing procedure, which is the same as fabricating the 2D gold nanodisk on plain GaN substrate, but here we coated a 150-nm-thick chromium (Cr) film as an etching mask after coating the 50-nm-thick gold film. After removing the remaining resist and using the Cr/Au nanodisks as the etching mask, an inductive coupled plasma reactive ion etching (ICPRIE) system was utilized to etch the uncovered GaN substrates as nanorod substrates with different rod-lengths, which were determined

19

by the etching depths. Finally we removed the chromium masks by chromium etchant (Cr7). Fig. 2.5 shows SEM image of our fabricated sample with different periodicities and rod lengths, while the diameter of gold nanodisks are all closed to 150 nm.
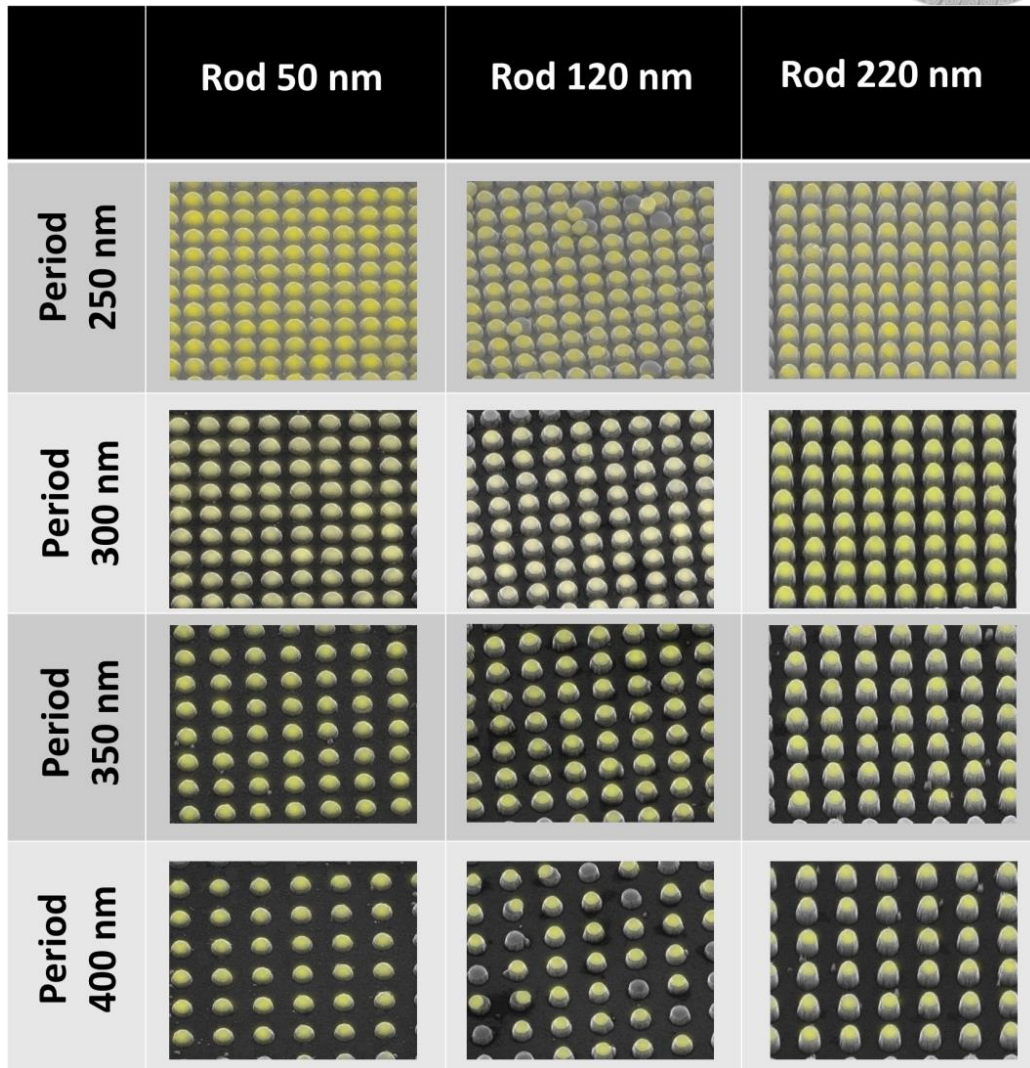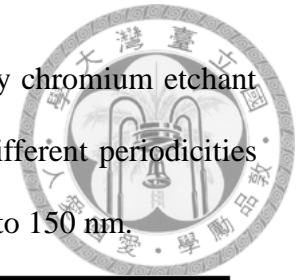
Figure 2.5 SEM images of the fabricated gold nanodisk arrays on top of GaN nanorod substrates with different periodicities and rod lengths.

To understand how the length of the nanorod affects the plasmonic coupling between gold nanodisks, the extinction spectra of the fabricated samples were measured. As shown in Fig. 2.6(a)-(c), the red-shift effect of the SPP-resonant wavelength by

increasing periodicity is decreased when the length of the GaN nanorod array was increased to 50 nm. This result suggests that nanorod substrate begin to suppress the dipolar coupling effect; however, the suppression is mild. By increasing rod length to 120 nm and 220 nm (Figs. 2.6(b), (c)), the trend of the wavelength shift, either an increase or decrease with periodicity, was no longer observed. This result indicates that the dipolar coupling effect among nanodisks is fully suppressed by the long-nanorod substrate, and LSPs are thus excited. It is worth noting that the plasmon-resonant wavelength of the nanodisk array on a nanorod array is blue shifted in contrast to its counterpart on a plain substrate. This effect can be explained by the fact that the nanorod structure reduces the effective refractive index of the substrate, and therefore, results in the blue-shifted resonant wavelength [22].
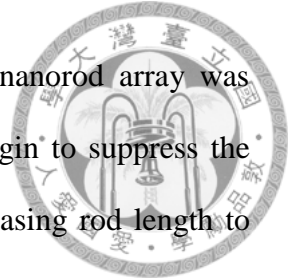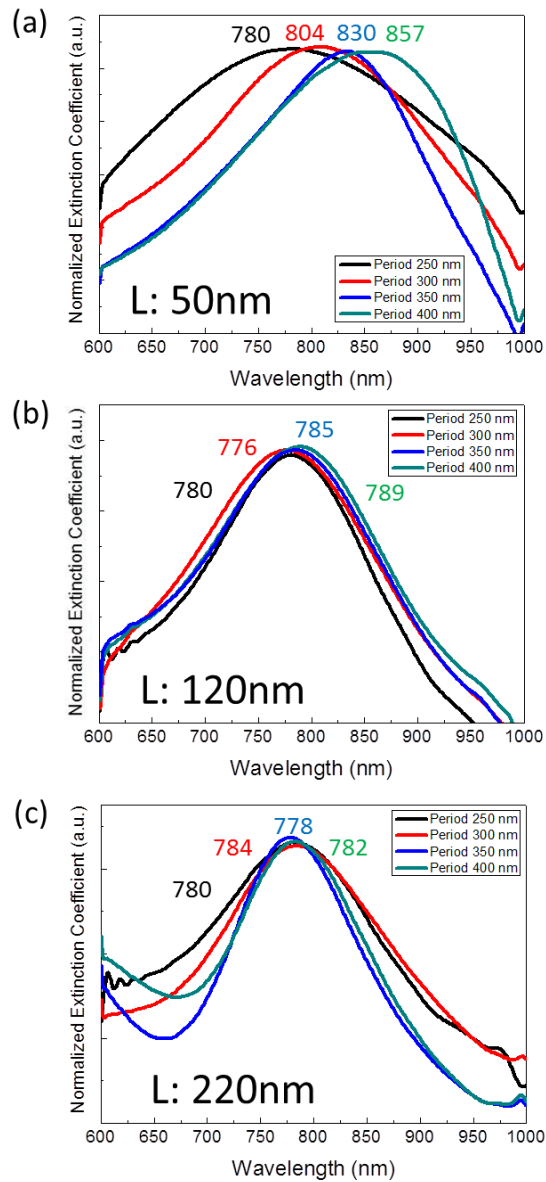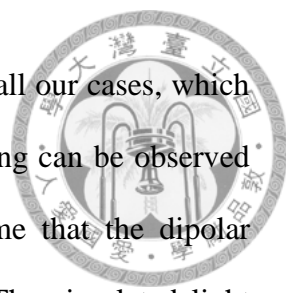
Figure 2.6 Experimentally measured normalized extinction spectra of the gold nanodisk arrays with different periods (a) on 50 nm, (b) 120 nm, and (c) 220 nm long GaN nanorod arrays.

To double confirm that the coupling between each disk is fully suppressed by the nanorod, we calculated the optical energy field distribution in the nanodisk arrays both on plain substrate and nanorod substrate. However, we only present the simulation of

the array with 250 nm periodicity as it is the shortest period among all our cases, which leads to the strongest coupling. If suppression of the dipolar coupling can be observed on the nanorod array with this period, we can then safely assume that the dipolar coupling effect will also be suppressed in the other three cases. The simulated light wave incident on the gold nanodisk is x-polarized (as defined in Fig. 2.7), and its wavelength corresponds to the peak wavelength of our extinction spectrum. Fig 2.7 shows the energy field distribution, whose polarization (E_z) is perpendicular to the surface of the substrate, excited by the incident light. Only the E_z field intensity is displayed as it is associated with plasmonic field [14]. It can be seen that the E_z intensity in the gold nanodisk array on a plain substrate is weak since the excited field below the gold nanodisk can extend through the substrate between disks. This effect induces the dipolar coupling, which leads to the strong period dependency. When the rod length is increased from 0 to 50 nm, part of the SPP field is confined inside the nanorod because of an abrupt change in the refractive index at the interface between GaN nanorods and air. Such a change can prevent field penetration through the nanorod/air interface in the lateral direction. However, part of the field still reaches the substrate and thus contributes to the dipolar coupling. Therefore, the length of the rod needs to be sufficiently long to prevent energy-field leakage through the substrate. After increasing the rod length to 120 nm and 220 nm, most of the field is now confined in the nanorod, and the period dependency is thus strongly suppressed. Our simulation thus indicates that the nanorod array with a sufficiently long rod length can effectively confine the light field inside the nanorod both in the lateral and longitudinal directions.
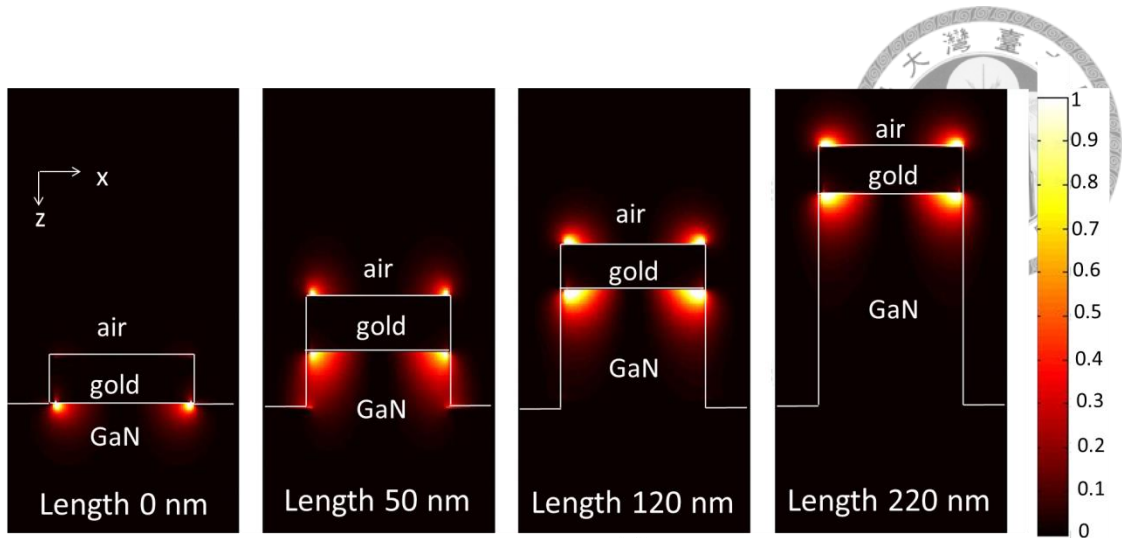
Figure 2.7 Simulated energy field distributions of gold nanodisk arrays with a 250 nm period on nanorod substrate with different rod lengths.

Furthermore, we measured the extinction spectra of gold nanodisk arrays on the nanorod substrate (L= 220 nm) and plain substrate at different incident angles of light to verify the LSP dominant behavior in long nanorods. Fig. 2.8 summarizes the peak wavelengths of the measured extinction spectra as a function of incident angle. The SPP-resonant wavelength on a plain substrate shifted from 814 nm to 850 nm when the angle of incident light was changed. However, the resonant wavelength of the gold nanodisk on top of the 220 nm-nanorod substrate remained constant at around 778 nm. Since the group velocity of LSPs is zero, this angularly independent characteristic further confirms the excitation of LSPs inside the nanorod [23, 24].
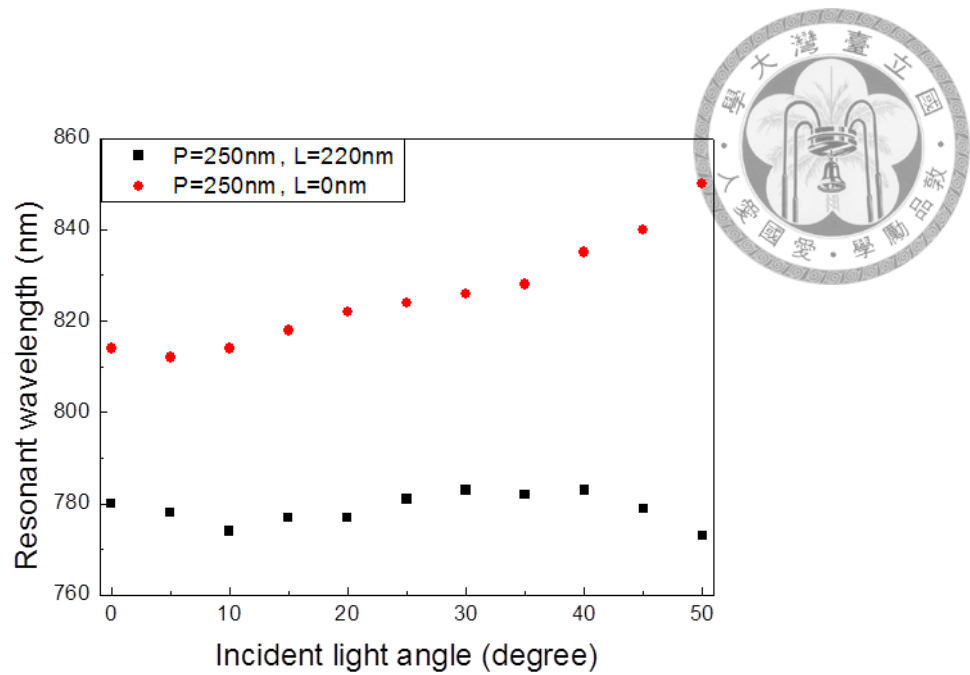
Figure 2.8 Peak wavelengths of measured extinction spectra of gold nanodisk array on plain substrate and nanorod substrate at different incident angles of light.

In this chapter, we discussed the plasmonic behavior from 1-D gold nanograting to 2-D gold nanodisk on plain substrate and on nanorod substrate. Our results indicate that gold nanodisk on top of GaN nanorod could confine the plasmonic field and induce LSPs. Such LSPs field may increase the detection sensitivity due to the intense plasmonic field. Furthermore each gold nanodisk acts like an independent detector by suppressing the coupling effect, which suggests that 2-D gold nanodisk array on top of GaN nanorod substrate as a great candidate for future hypersonic imaging system.

Reference

[1] A. G. Brolo, R. Gordon, B. Leathem, and K. L. Kavanagh, Langmuir **20**, 4813-4815 (2004).

[2] J. Wang, J. Wu, and C. Guo, Opt. Lett. 32, 719–721 (2007).

[3] H.-P. Chen, Y.-C. Wen, Y.-H. Chen, C.-H. Tsai, K.-L. Lee, P.-K. Wei, J.-K. Sheu, and C.-K. Sun, Appl. Phys. Lett. 97, 201102 (2010).

[4] C. Bruggemann, J. Jager, B. A. Glavin, V. I. Belotelov, I. A. Akimov, S. Kasture, A. V. Gopal, A. S. Vengurlekar, D. R. Yakovlev, A. V. Akimov, and M. Bayer, Appl. Phys. Lett. 101, 243117 (2012).

[5] S.-C. Yang, H.-P. Chen, H.-H. Hsiao, P.-K. Wei, H.-C. Chang, and C.-K. Sun, Opt. Express 20, 16186 (2012).

[6] C. Bruggemann, A. V. Akimov, B. A. Glavin, V. I. Belotelov, I. A. Akimov, J. Jager, S. Kasture, A. V. Gopal, A. S. Vengurlekar, D. R. Yakovlev, A. J. Kent, and M. Bayer, Phys. Rev. B. 86, 121401 (2012).

[7] P.-A. Mante, H.-Y. Chen, M.-H. Lin, Y.-C. Wen, S. Gwo, and C.-K. Sun, Appl. Phys. Lett. 101, 101903 (2012).

[8] S. A. Maier, Plasmonics: Fundamentals and Applications (Springer, New York, 2007), p. 26.

[9] M. G. Moharam and T. K. Gaylord, J. Opt. Soc. Am. **71**, 811 (1981).

[10] Yee, IEEE Trans. Antenn. Propag. 14, 302 (1966).

[11] P. B. Johnson and R. W. Christy, Phys. Rev. B **6**, 4370 (1972).

[12] S. Adachi, Optical Constants of Crystalline and Amorphous Semiconductors: Numerical Data and Graphical Information (Springer, New York, 1999), p. 177.

[13] Y. Cui and S. He, Opt. Lett. **34**, 16-18 (2009).

[14] S. A. Maier, Plasmonics: Fundamentals and Applications (Springer, New York, 2007), p. 29.

[15] V. A. Markel, J. Mod. Opt. **40**, 2281 (1993).

[16] L. L. Zhao, K. L. Kelly, andG.C. Schatz, J. Phys. Chem. B **107**, 7343 (2003).

[17] C. L. Haynes, A. D. McFarland, L. L. Zhao, R. P. Van Duyne, G. C. Schatz, L. Gunnarsson, J. Prikulis, B. Kasemo, and M. J. Kall, Phys. Chem. B **107**, 7337 (2003).

[18] J. Aizpurua, P. Hanarp, D. S. Sutherland, M. Käll, G. W. Bryant and F. J. García de Abajo, Phys. Rev. Lett. **90**, 057401 (2003).

[19] S.-C. Yang, P.-K. Wei, T.-W. Liao, M.-L. Tsai, P.-A. Mante, Y.-R. Huang, I-J. Chen, H.-Y. Chen, and C.-K. Sun, in Technical Digest of Conference on Lasers and Electro-Optics (CLEO2013:Laser Science to Photonic Applications), paper JTu4A.63, San Jose, CA, 2013.

[20] S.-C. Yang, P.-K. Wei, H.-H. Hsiao, P.-A. Mante, Y.-R. Huang, I.-J. Chen, H.-C. Chang, and C.-K. Sun, Appl. Phys. Lett. **105**, 211103 (2014).

[21] J. Homola , S. S. Yee , and G. Gauglitz , Sens. Actuators, B **54**, 3 (1999).

[22] M. D. Malinsky, K. L. Kelly, G. C. Schatz, and R. P. Van Duyne, J. Phys. Chem. B **105**, 2343 (2001).

[23] C.-M.Wang, Y.-C. Chang, M.-W. Tsai, Y.-H. Ye, C.-Y. Chen, Y.-W. Jiang, Y.-T. Chang, S.-C. Lee, and D.-P. Tsai, Opt. Express **15**, 14673 (2007).

[24] M. N. Abbas, C.-W. Cheng, Y.-C. Chang, M.-H. Shih, H.-H. Chen and S.-C. Lee, Appl. Phys. Lett. **98**, 121116 (2011).

Chapter 3

Confined Acoustic Vibration of Gold Nanodisk

3.1 Introduction

In previous chapter, we have investigated the plasmonic behavior in 1-D gold nanograting, 2-D gold nanodisks array on GaN plain substrate and nanorod substrate. Our results indicate that gold nanodisk on top of GaN nanorod array may be served as a good hypersonic detector due to the excitation of LSPs. Fig. 3.1 shows the scheme of hypersonic detection by this structure, hypersonic waves propagated from substrate are first guided by GaN nanorod and detected by coupling to vibrational modes of the detector, which are gold nanodisk in our case [1, 2]. However, due to the spatial confinement, not only electrons but also acoustic phonons would be quantized in the nanostructures such as GaN nanorod and gold nanodisk, which leads different behavior of acoustic waves in the nanostructure. For example, the abnormality of thermal conductance in nanostructure compared to the bulk material is observed [3-7]. Therefore the hypersonic behavior in these nanostructures should be investigated before discussing the interaction between plasmons and hypersonic pulse. In this chapter, the confined acoustic modes (CAMs) of gold nanodisk and the acoustic guiding mode (AGM) of GaN nanorod would be studied, which may help us to understand the possible detection frequency of the hypersonic waves.
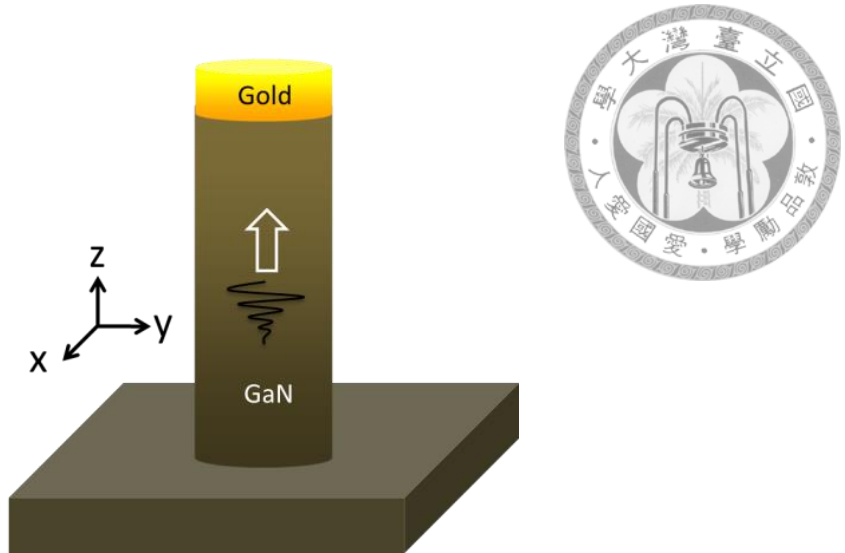
Figure 3.1 Schematic showing the detection of hypersonic waves by gold nanodisk on top of GaN nanorod.

3.2 Confined Acoustic Vibrations of Gold Nanodisk

As we mentioned above, hypersonic waves with specific frequencies can couple to the vibrational modes of gold nanodisk. Basically in this case, gold nanodisk can be treated as a micro resonator for hypersonic waves. Once the frequencies of hypersonic waves match the resonant frequencies of the resonator, acoustic phonons would be confined in the resonator and the survival time of the acoustic phonons depends on the phonon scattering at the interface [8, 9], acoustic impedance of the attached material [10]. In this section, behavior of acoustic phonons in gold nanodisk is calculated by Pochammer-Chree Theory, which is used to describe the propagation of axisymmetric, torsional and flexural waves in the cylinder structure [11, 12]. The following equation is the well-known Pochammer-Chree equation:

$$\frac{2p}{a}(q^2+k^2)J_1(pa)J_1(qa) - (q^2-k^2)^2J_0(pa)J_1(qa) - 4k^2pqJ_1(pa)J_0(qa) = 0 \text{ (1)}$$

Where a is the radius of the nanodisk, J is the Bessel function, $p = [\left(\frac{\omega}{v_L}\right)^2 - k^2]^{\frac{1}{2}}, q =$

$[\left(\frac{\omega}{V_T}\right)^2 - k^2]^{\frac{1}{2}}$, ω and k are the angular frequency and wavenumber of the acoustic phonons, while V_L and V_T are the longitudinal and transverse sound velocity. By solving this equation, we can obtain the dispersion curves of acoustic phonons in the cylinder structure. By considering the longitudinal and transverse sound velocity in gold as 3240 m/s and 1820 m/s, Fig. 3.2(a) shows the calculated result of the acoustic phonon mode in gold nanodisk with 150 nm diameter, which is the size we discussed in the previous chapter. When k=0, the slope of these dispersion curves equal to zero, which suggests that the group velocity of acoustic phonons is zero. These acoustic phonons are thus not able to escape from the resonator and we called these modes as CAMs. The arrows indicate frequencies of CAMs of gold nanodisk. The validity can further be verified numerically. Fig. 3.2(b) shows calculated eigen frequencies and the corresponding displacement field distribution of CAMs of gold nanodisk (calculated by the finite element method, COMSOL Multiphysics, COMSOL, Inc.). The obtained frequencies are in a good agreement with frequencies predicted by Pochammer-Chree Theory. This result basically indicates that even though we launched the hypersonic pulse to the gold nanodisk on top of GaN nanorod, not all frequency components can be detected. The detected frequencies of the gold nanodisk would be limited to the frequencies of CAMs.
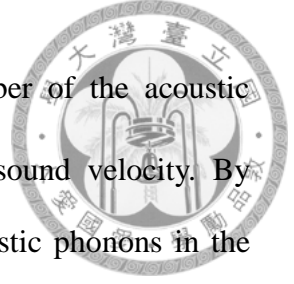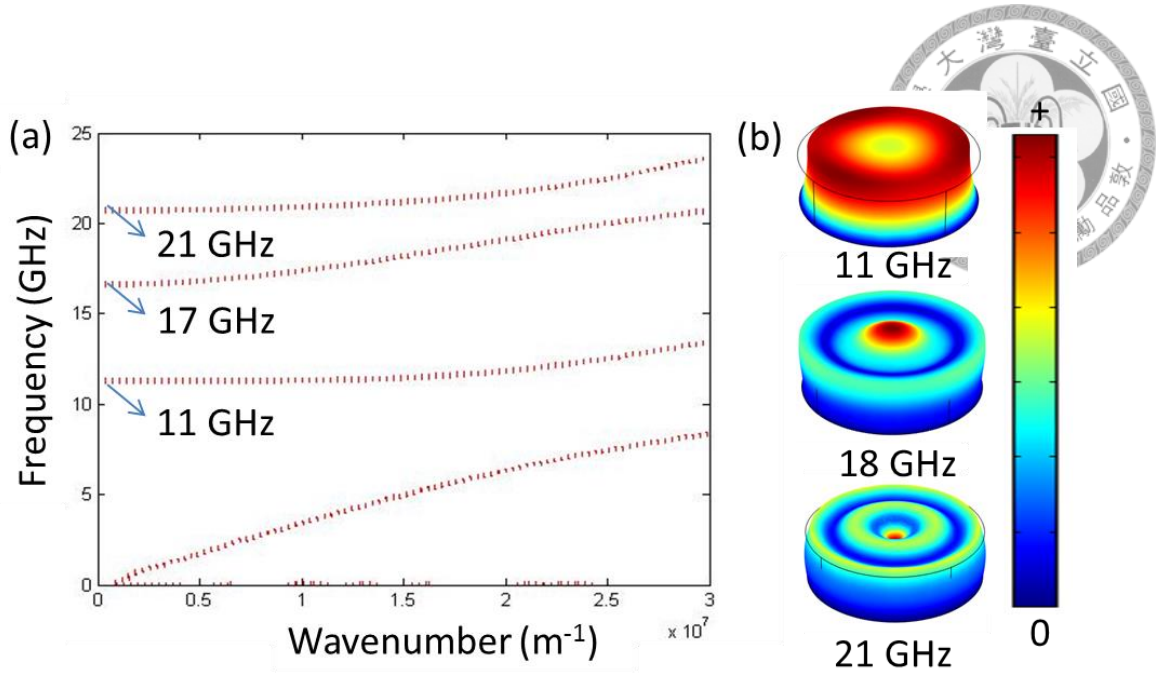
Figure 3.2 (a) The dispersion curves of acoustic phonon modes in gold nanodisk calculated based on Pochammer-Chree Theory (b) The eigen frequencies and the corresponding displacement field distributions of CAMs of gold nanodisk.

3.3 Acoustic Guiding Modes of GaN Nanorod

In our case, GaN crystal is grown on c-plane, which is anisotropic compared to the gold nanodisk in the previous section. The Pochammer-Chree theory is thus not able to calculate the phonon behavior in GaN nanorod. To solve this problem, Migliori and Visscher used simple basis function to compute the phonon mode of anisotropic elastic body. This method is also called Resonant Ultrasound Spectroscopy (RUS). By using the xyz-algorithm developed for the RUS method [13, 14], the Lagrangian of the system can be expressed as:

$$L = \frac{1}{2} \int_V \left[\frac{1}{2} \rho \omega^2 u_i u_i - C_{ijkl} \frac{\partial u_i}{\partial x_j} \frac{\partial u_k}{\partial x_l} \right] dV \quad (2)$$

where u_i is the lattice displacement component, C_{ijkl} is the elastic stiffness tensor, ρ is the

31

mass density, and ω is the angular frequency. The displacement fields in terms of a complete set of functions Φ_α can be expanded as:

$$u_i = \sum_\alpha a_{i\alpha}\Phi_\alpha \quad (3)$$

Then, the basis function that is a power of the x, y, and z directions is:

$$\Phi_\alpha = \left(\frac{x}{r}\right)^m \left(\frac{y}{r}\right)^n e^{iqz} \quad (4)$$

where r is the radius of the nanorod and q is the longitudinal wave vector of the acoustic phonon modes. By substituting the elastic stiffness tensor of the material into eq. (2), we were able to calculate the dispersion curves of the acoustic phonon modes for the anisotropic case, and thus for GaN.

Figure 3.3(a) shows the calculated dispersion curves of GaN nanorod (black-solid lines) as well as the dispersion curves of gold nanodisk (red-dash lines). Theoretically acoustic energy coupling should occur at the interactions of the dispersion curves in order to maintain the momentum conservation. Frequencies marked by red crosses thus indicate the possible coupling frequencies between the fundamental AGM of GaN nanorod and the CAMs of gold nanodisk. Fig. 3.3(b) shows the displacement field distributions of the fundamental AGM in GaN nanorod and CAMs of gold nanodisk on the x-y plane at the coupling frequencies. (The definition of the coordinate is shown in Fig. 3.1). One can observe that the displacement field of fundamental AGM is mainly on the x-y plane and the maximum of the field is closed to the edge of the nanorod. Such displacement field agrees well with the fundamental CAM of gold nanodisk (12 GHz). However, for 19 GHz case, the displacement field on the edge of the nanodisk is normal to the x-y plane. This result suggests that it is difficult to couple the fundamental AGM to 19 GHz CAM due to the fact that the directions of the maximum displacement fields of
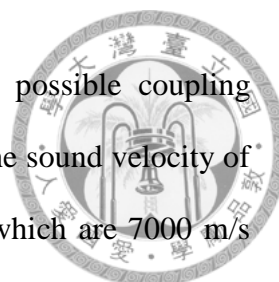
these two modes are normal to each other. Therefore the most possible coupling frequencies in our structure are 12 GHz and 22 GHz. Furthermore the sound velocity of 12 GHz and 22 GHz hypersonic waves in 150 nm GaN nanorod, which are 7000 m/s and 5000 m/s, can be derived from the dispersion curve in Fig. 3.3(a). Since the longitudinal sound velocity in bulk GaN substrate is 8020 m/s, it will be more difficult for 22 GHz hypersonic waves to transmit from the bulk substrate into the nanorod due to the larger acoustic impedance mismatch. As a result, the design of our hypersonic array is intended to detect the 12 GHz hypersonic waves whose frequency is the same as the fundamental vibrational mode of the gold nanodisk.
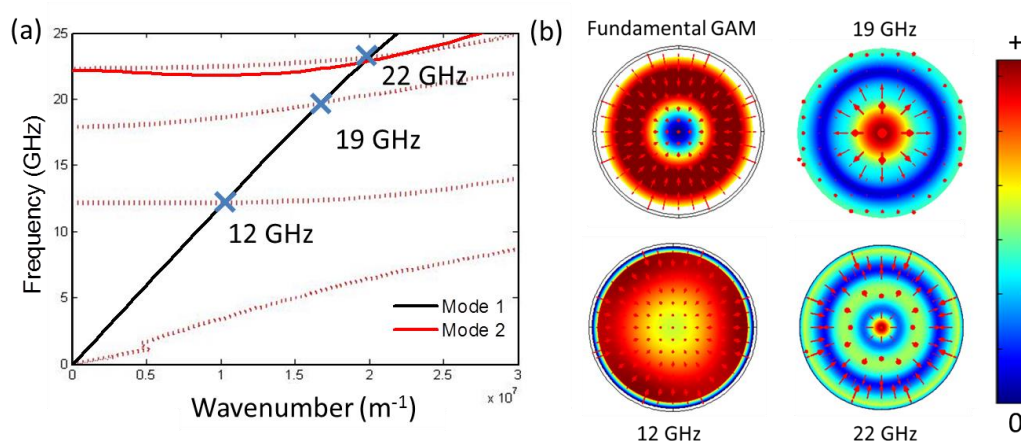
Figure 3.3 (a) The dispersion curves of acoustic phonon modes in GaN nanorod as well as in gold nanodisk with 150 nm diameter, the interactions suggest coupling frequencies of the hypersonic waves between GaN nanorod and gold nanodisk. (b) Calculated displacement field distributions of the three lowest CAMs in 150 nm gold nanodisk and the fundamental AGM in 150 nm GaN nanorod.

Reference

[1] T. R. Gururaja, W. A. Schulze, L. E. Cross, R. E. Newnham, B. A. Auld, and Y. J. Wang, IEEE Trans. Sonics Ultrason. **32**, 481 (1985).

[2] K. C. Cheng, H. L. W. Chan, C. L. Choy, Q. R. Yin, H. S. Luo, and Z. W. Yin, IEEE Trans. Ultrason. Ferroelectr. Freq. Control **50**, 1177 (2003).

[3] R. Chen, A. I. Hochbaum, P. Murphy, J. Moore, P. Yang, and A. Majumdar, Phys. Rev. Lett. **101**, 105501 (2008).

[4] A. I. Boukai, Y. Bunimovich, J. Tahir-Kheli, J.-K. Yu, W. A. Goddard III, and J. R. Heath, Nature **451**, 168-171 (2008).

[5] A. I. Hochbaum, R. Chen, R. Diaz Delgado, W. Liang, E. C. Garnett, M. Najarian, A. Majumdar, and P. Yang, Nature **451**, 163-167 (2008).

[6] N. Mingo, and D. A. Broido, Phys. Rev. Lett. **93**, 246106 (2004).

[7] J. Zou, J. Appl. Phys. **108**, 034324 (2010).

[8] E. T. Swartz and R. O. Pohl, Rev. Mod. Phys. **61**, 605 (1989).

[9] N. S. Shiren, Phys. Rev. Lett. **47**, 1466 (1981).

[10] S.-C. Yang, Y.-C. Wu, P.-A. Mante, C.-C. Chen, H.-P. Chen, H.-Y. Chou, M.-H. Shih and C.-K. Sun, Appl. Phys. Lett. **105**, 243101 (2014).

[11] P.-A. Mante, Y.-C. Wu, C.-Y. Ho, L.-W. Tu, and C.-K. Sun, Nano Lett. **13**, 1139 (2013).

[12] M. Redwood, Mechanical Waveguides (Pergamon Press, New York 1960), p. 135.

[13] W. M. Visscher, A. Migliori, T. M. Bell, and R. A. Reinert, J. Acoust. Soc. Am. **90**, 2154 (1991).

[14] R. G. Leisure and F. A. Willis, J. Phys.: Condens. Matter **9**, 6001 (1997).

Chapter 4

Interaction between Plasmons and Hypersonic Pulse

4.1 Introduction

So far, we have investigated the plasmonic behavior and possible detected frequencies of the proposed hypersonic detector. In order to utilize the plasmons as a hypersonic sensor, the interaction between hypersonic pulse and plasmons needs to be studied. In this chapter, the interaction between these two phenomena will be investigated by the femtosecond time resolved spectroscopy. Detailed descriptions of our experimental setup and results will be given later.

4.2 Interaction in 1-D Gold Nanogratings

Although 2-D gold nanodisks on top of GaN nanorod would be the ultimate choice for our hypersonic detector, we still begin our discussion from the 1-D gold nanogratings on GaN plain substrate, which is first described in chapter 2. Here we choose the nanogratings with 590 nm periodicity while the height and width of the slit are both 70 nm. Fig. 4.1(a) shows the transmission spectrum of the sample, which suggests that EOT occurred around 700 nm. Theoretically hypersonic pulse would modify the refractive index of the sample and shift the transmission spectrum. By choosing the probe wavelength closed to the maximum of the slope of the spectrum, such shift would induce the maximum of the transmission change (better detection sensitivity). Therefore the absolute value of the wavelength derivative of the measured transmission spectrum shown in Fig. 4.1(a) can roughly provide a guideline to estimate

the wavelength dependent transmission modulation strength induced by the refractive index change. From Fig. 4.1(a), 670 nm and 720 nm are two most sensitive wavelengths for EOT modulation. In order to study the field intensity distribution at these two wavelengths, we performed a FDTD [1] simulation to understand the field intensity distribution at 670 nm and 720 nm respectively. The refractive index values of gold and GaN were taken from [2] and [3], respectively. Plane waves are incident from the substrate side with TM polarization (x-direction in Fig. 4.1(b)). From the FDTD simulations shown in Fig. 4.1(b), we can observe that the SPP field exists mainly at gold/GaN interfaces for the 720 nm case. However, the SPP field exists only at gold/air interface for the 670 nm case. Since there is no field below the gold grating for the 670 nm case, the SPP field is only sensitive to the environment change above the gold. In order to acoustically modulate the refractive index of GaN and to maximize the EOT modulation through the opto-acoustic effect [4], we chose the operating probe wavelength as 720 nm.
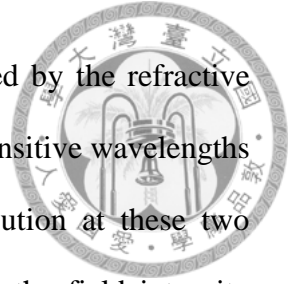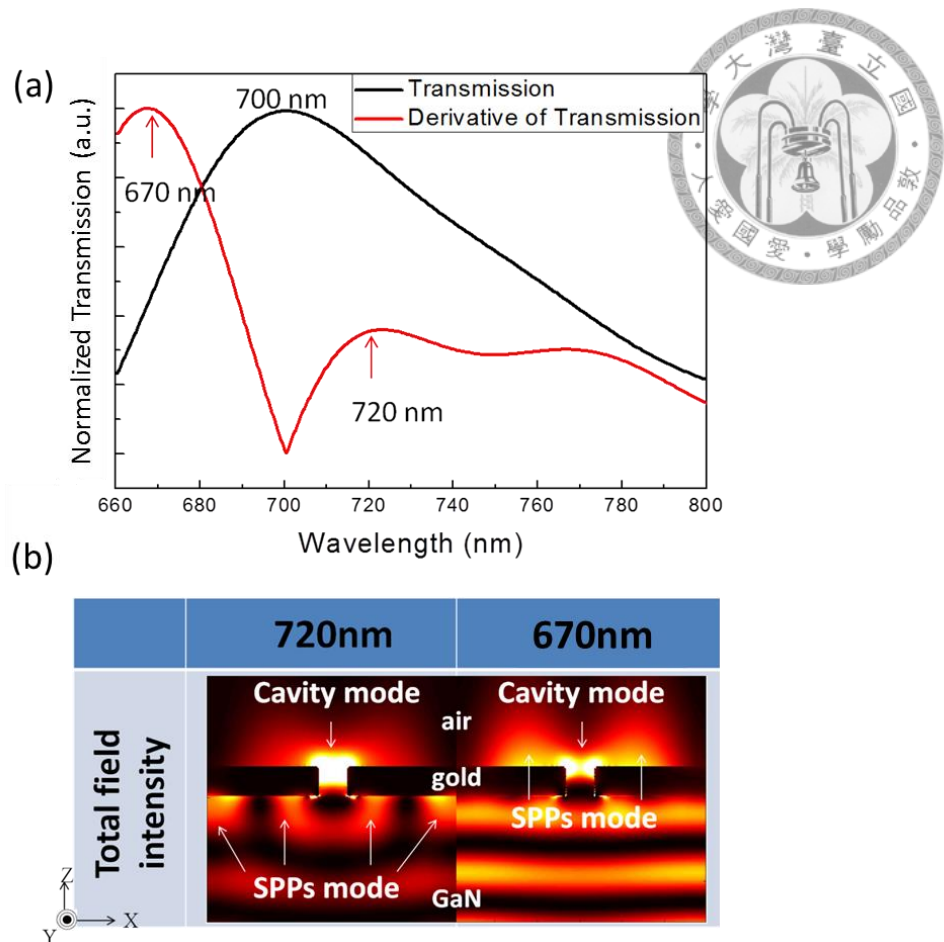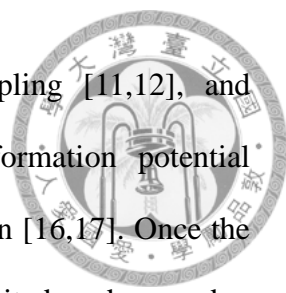
Figure 4.1 (a) Experimental normalized transmission spectrum and the absolute value of its derivative of the studied sample. (b) Simulated results showing the energy field distribution at 720 nm and 670 nm wavelength respectively.

A femtosecond time resolved spectroscopy [5–7] was used to generate both hypersonic pules and EOT in gold nanogratings. The light source of our spectroscopy is a 720 nm mode-locked Ti:sapphire laser (Coherent Mira 900) with a 100 fs pulse width and a 76 MHz repetition rate. As we mentioned in chapter 1, there are two laser beams in the system. One of them is pump beam, which is used to excite the hypersonic pulse in GaN. Another one is probe beam, which detects the pump-induced optical change. There are many mechanisms responsible for the optical excitation of hypersonic pulse,

including thermal expansion [8–10], deformation potential coupling [11,12], and piezoelectric coupling [13–15]. For a GaN single crystal, deformation potential coupling is the dominant mechanism for hypersonic pulse generation [16,17]. Once the above-bandgap pump light was absorbed, free carriers were excited and caused a mechanic strain/stress in the semiconductor [18]. Since our GaN crystal is grew on c-plane sapphire substrate, the optically induced mechanic strain/stress could launch hypersonic pulse from the GaN/sapphire interface. The pulse width of the hypersonic pulse is thus equal to the twice of the penetration depth of pump beam in the GaN single crystal, which was 150 nm.

In order to generate hypersonic pulse in GaN, the pump beam is set to be above the bandgap energy of GaN. As shown in Fig. 4.2, the mode-locked laser beam is thus first passed through the beta barium borate (BBO) crystal in order to generate frequency-doubled pump beam (360 nm) for generating hypersonic pulse in GaN. The unconverted laser beam is chose as probe beam (720 nm), which is used to generate EOT and detect the pump-induced optical change in the sample. These two laser beams are separated by the dichromatic mirror. The optical path between pump beam and probe beam can be modified by the delay stage. Probe beam is then passed through the telescope in order to make sure that both pump beam and probe beam will be focused at the sample. Since pump beam is modulated by an AO modulator, the optical change detected by probe beam would also be modulated by the same frequency. Therefore the transmitted probe beam collected by the detector is sent to the lock-in amplifier for demodulation. The diameters of pump and probe beams at focus were 10 µm and 25 µm, respectively. With a nanostructure area covering 300 µm×300 µm, the focused laser spot sizes were much smaller than the nanostructure size and we made sure that all the

measured signals were through the nanostructure. The pump and probe average powers

at the sample surface were 50 mW and 10 mW, respectively.
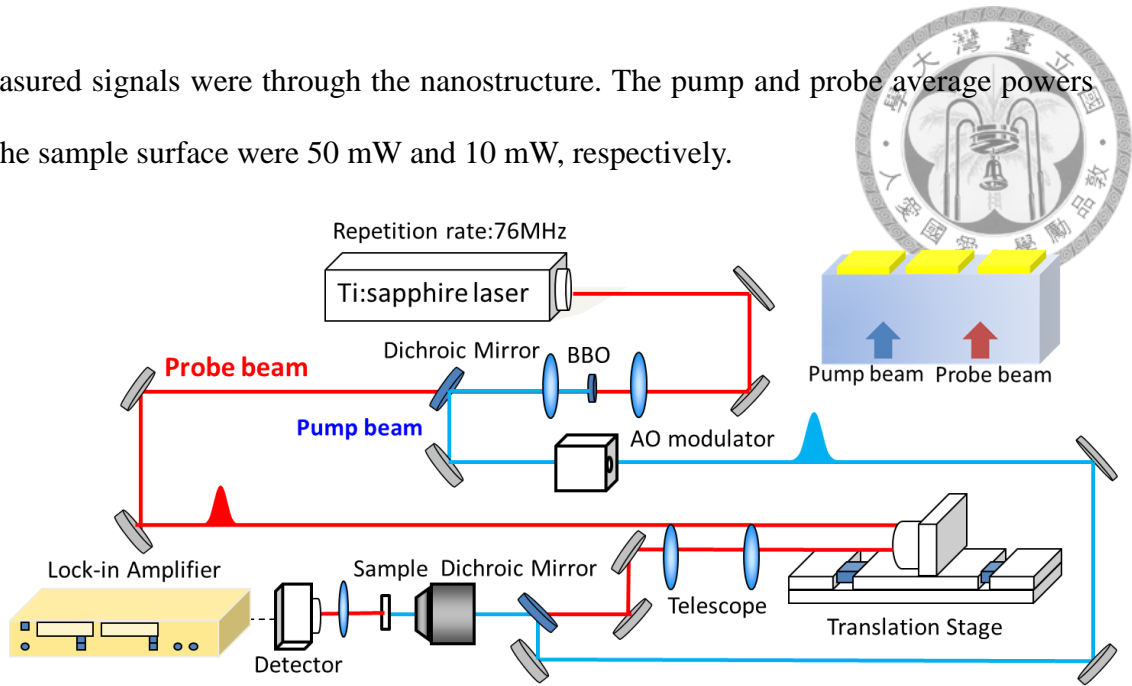
Figure 4.2 Schematic showing of optical transmission type of femtosecond time

resolved spectroscopy (inset: pump beam and probe beam are incident from the bottom

of the sample).

With the femtosecond time resolved spectroscopy, excited free carriers generated

stress with a mechanic strain on the order of 10^{-4}, which is calculated based on Eq. (18)

in [16]. Fig. 4.3(a) shows the transient transmissions change with TE polarized probe

beam and with TM polarized probe beam measured in different experiments. The

transient transmission change at zero time delay is due to carrier excitation by the pump

beam and the exponentially-decaying background is caused by carrier relaxation. The

transient transmission difference in the TM case (x-direction in Fig. 4.1(b)) is higher

than the TE case (y-direction in Fig. 4.1(b)), which suggests that EOT is induced by TM

polarized incident light. At the same time, a bipolar shaped signal between 400 ps and

500 ps appears in the TM case for all experimental traces. Fig. 4.3(b) shows the

carrier-dynamics background-removed bipolar shaped signal from Fig. 4.3(a). Based on

the delay time in Fig. 4.3(b), we are able to calculate the position of the hypersonic pulse in GaN. Fig. 4.3(c) shows the calculated result, which indicates that the corresponding delay time of this bipolar shaped signal agrees well with the acoustic traveling time from the GaN/sapphire interface to enter and leave the SPPs field below the gold respectively [19]. Based on the measurement, we observed that the transmission was first decreased and then increased by the hypersonic pulse. The transmission change induced by hypersonic pulse was close to zero at ~465 ps due to the fact that the center of the hypersonic pulse was near gold/air interface. The hypersonic pulse was then reflected from this interface with a sign change [20], which causes the sign change of the refractive index change and thus the sign change of the transmission modulation.
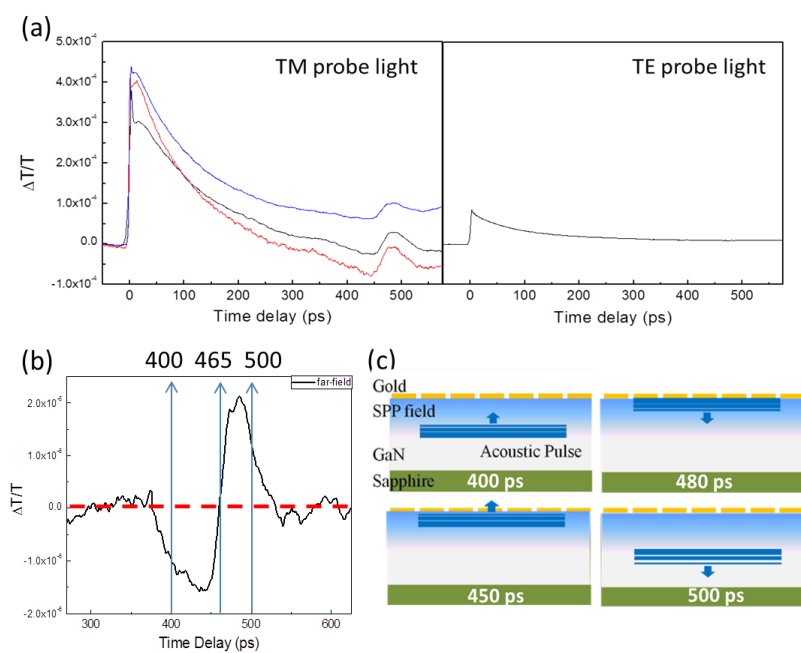
Figure 4.3 (a) Experimentally measured transient transmission in TM and TE polarized incident light. (b) Background removed transient transmission change between 300 ps to 600 ps. (c) Schematic showing the locations of hypersonic pulse at different time delays.

4.3 Interaction in 2-D Gold Nanodisks Arrays

In the previous section, we have demonstrated that the SPPs in 1-D gold nanogratings enable the detection of the bipolar-liked signal, which suggests the enhanced detection of the propagated hypersonic pulse in GaN. However this structure limits the detection in 1-D. As we mentioned in section 2.3, we modified our structure into 2-D gold nanodisk arrays to expand our detection in another dimension. Meanwhile the plain GaN substrate was also modified into nanorod arrays to suppress the dipolar coupling effect among neighbored gold nanodisk and excite LSPs. This LSP-based sensor suggests the better sensitivity of the acoustic detection owing to the strong concentration of the plasmonic field [21]. In order to verify our suggestion, we first investigate the interaction between the CAMs of gold nanodisk and LSPs as well as SPPs.

4.3.1 Interact with Confined Acoustic Modes in Gold Nanodisk

We chose the nanodisk arrays with a period of 250 nm, but with a different lengths since closer-packed arrays maximize the signal-to-noise ratio. Based on the discussion of section 2.3, rod length longer than 120 nm could excite LSPs in the nanorod array. We thus compare the extinction spectra between different rod length cases (Fig. 4.4(a)). We observed that more light is absorbed by gold nanodisks on rods because of the excitation of LSPs. To enhance the detection of acoustic vibrations, the wavelength of the probe beam was chosen to be 720 nm, which was near the maximum of the derivative of the extinction spectrum.
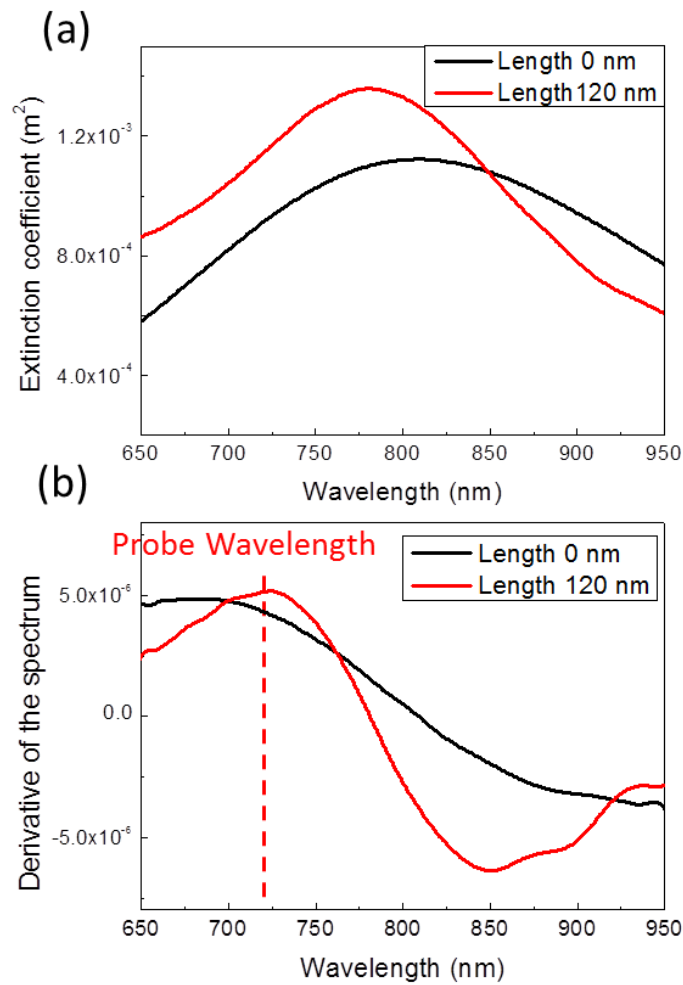
Figure 4.4 (a) Experimental extinction spectra and (b) the derivative of spectra of gold nanodisk on plain substrate and 120 nm nanorod substrate.

As shown in the inset of Fig. 4.5, both pump beam and probe beam were incident from the side of the gold nanodisks to directly generate and detect the CAMs of gold nanodisk. In order to avoid the absorption of GaN nanorod, the wavelength of the pump beam was also 720 nm. Therefore the BBO crystal was removed from the experimental setup. Furthermore the telescope, which was used to compensate the dichromatic aberration due to different wavelengths between pump and probe beam, was also

removed. The reflected probe beam from the gold nanodisk was collected by the detector. The diameters of the pump and probe beams at focus were respectively 20 μm and 30 μm, which are also much smaller than the area covered with nanostructures (300 μm×300 μm). The average power of the pump and probe at the sample surface were 40 mW and 4 mW, respectively.
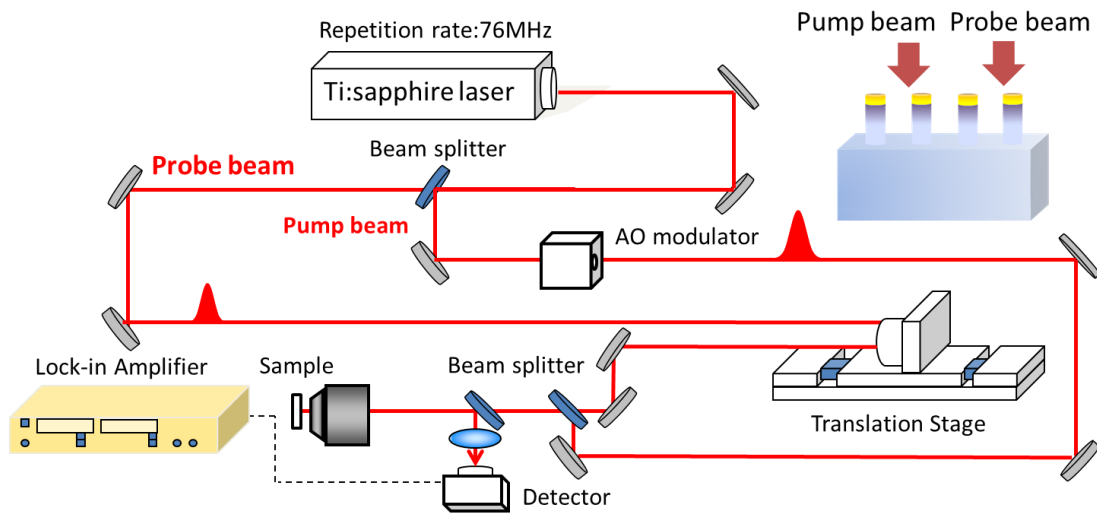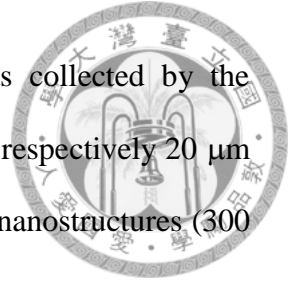
Figure 4.5 Schematic showing of optical reflection type of femtosecond time resolved spectroscopy (inset: pump beam and probe beam are incident from the top of the sample).

Fig. 4.6(a) shows the transient reflection changes of the gold nanodisk arrays with 250 nm periodicity on GaN nanorod arrays with two different rod lengths after removing the background, while the inset shows the original transient reflection changes. From Fig. 4.4(a), the extra pump light absorbed by the LSPs at 720 nm was calibrated, and subsequently, stronger optical reflection oscillations were observed for the gold nanodisks on the nanorod substrate. Combined with our above discussion, we attribute this difference to the different probe sensitivities because a stronger field

intensity of LSPs is excited in the samples on top of nanorod arrays. This strong LSP field enhanced the detection sensitivity of the probe beam compared to those on top of a plain substrate. The time-frequency analysis was adopted to analyze the frequency of the measured change in transient reflection as a function of time. In Fig. 4.6(b), oscillation signals at 11, 18, and 22 GHz were clearly observed for the 120 nm rod length substrate. However, only oscillations at 11 GHz were obvious in the plain substrate. Comparing to the acoustic dispersion curve of a single gold nanodisk with a 150 nm diameter, which was calculated based on the Pochammer Chree Theory [22, 23] (Fig. 3.2(a)), theoretically expected frequencies of the CAMs of the gold nanodisk are 11 GHz, 17 GHz, and 21 GHz. Our experimental observation and the calculation are in good agreement with these values. We thus attribute the frequencies observed in the experiment to the CAMs of the gold nanodisk. Furthermore it can be seen that, weak, higher-order vibrations of the gold nanodisk become observable because of the stronger LSP field intensity in the nanorod. This result verifies that the well-confined LSP field in the nanorod indeed increases the sensitivity of hypersonic detection.
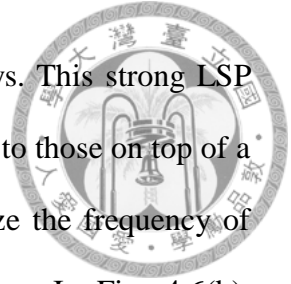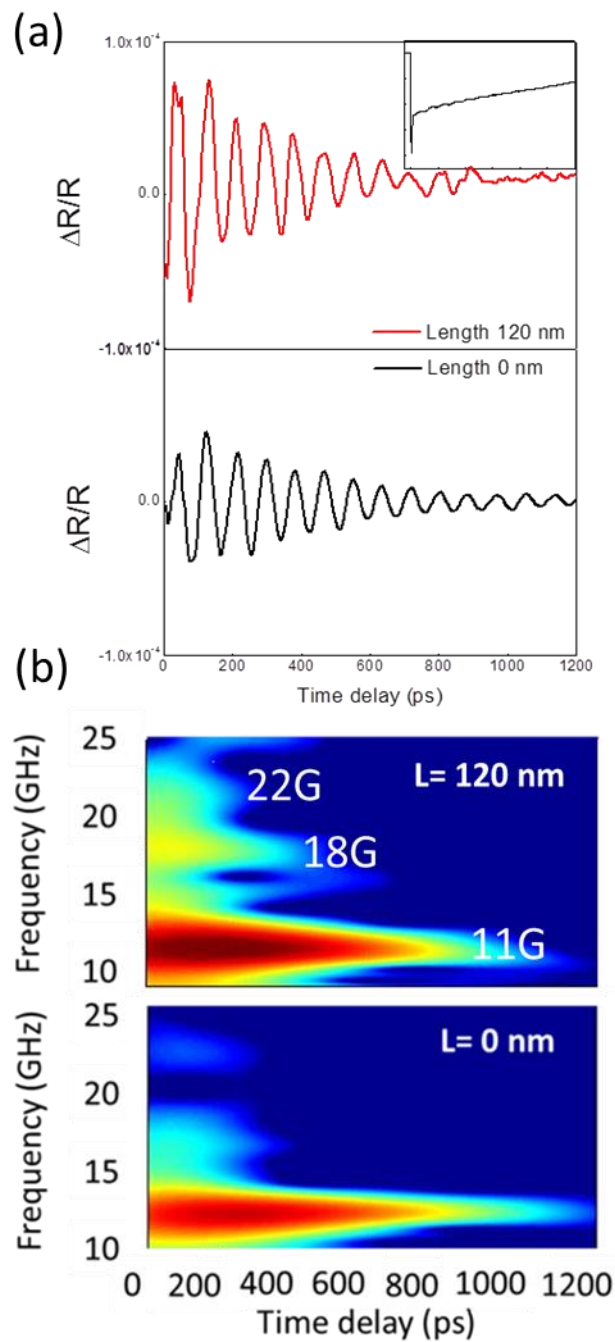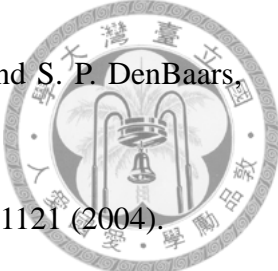
Figure 4.6 (a) Transient reflection changes of gold nanodisk arrays with 250 nm periodicity and different rod length. (b) Time-frequency analysis of transient reflection change in Fig. 4.6(a). Higher-order vibrational modes of gold nanodisk are observable for 120 nm rod length substrate.

Reference

[1] Yee, IEEE Trans. Antenn. Propag. **14**, 302 (1966).

[2] P. B. Johnson and R. W. Christy, Phys. Rev. B **6**, 4370–4379 (1972).

[3] S. Adachi, Optical Constants of Crystalline and Amorphous Semiconductors: Numerical Data and Graphical Information (Springer, New York, 1999), p. 177.

[4] D. Gérard, V. Laude, B. Sadani, A. Khelif, D. Van Labeke, and B. Guizal, Phys. Rev. B 76, 235427 (2007).

[5] Y.-K. Huang, G.-W. Chern, C.-K. Sun, Y. Smorchkova, S. Keller, U. Mishra, and S. P. DenBaars, Appl. Phys. Lett. **79**, 3361–3363 (2001).

[6] K.-H. Lin, G.-W. Chern, C.-T. Yu, T.-M. Liu, C.-C. Pan, G.-T. Chen, J.-I. Chyi, S.-W. Huang, P.-C. Li, and C.-K. Sun, IEEE Trans. Ultrason. Ferroelectr. Freq. Control **52**, 1404–1414 (2005).

[7] K.-H. Lin, C.-M. Lai, C.-C. Pan, J.-I. Chyi, J.-W. Shi, S.-Z. Sun, C.-F. Chang, and C.-K. Sun, Nat. Nanotechnol. **2**, 704–708 (2007).

[8] C. Thomsen, J. Strait, Z. Vardeny, H. J. Maris, J. Tauc, and J. J. Hauser, Phys. Rev. Lett. **53**, 989–992 (1984).

[9] C. Thomsen, H. T. Grahn, H. J. Maris, and J. Tauc, Phys. Rev. B Condens. Matter **34**, 4129–4138 (1986).

[10] H.-N. Lin, R. J. Stoner, H. J. Maris, and J. Tauc, J. Appl. Phys. **69**, 3816–3822 (1991).

[11] A. Bartels, T. Dekorsy, H. Kurz, and K. Köhler, Phys. Rev. Lett. **82**, 1044–1047 (1999).

[12] O. B. Wright and V. E. Gusev, Appl. Phys. Lett. **66**, 1190–1192 (1995).

[13] C.-K. Sun, J.-C. Liang, and X.-Y. Yu, Phys. Rev. Lett. **84**, 179–182 (2000).

46

[14] C.-K. Sun, J.-C. Liang, C. J. Stanton, A. Abare, L. Coldren, and S. P. DenBaars, Appl. Phys. Lett. **75**, 1249–1251 (1999).

[15] G.-W. Chern, K.-H. Lin, and C.-K. Sun, J. Appl. Phys. **95**, 1114–1121 (2004).

[16] S. Wu, P. Geiser, J. Jun, J. Karpinski, and R. Sobolewski, Phys. Rev. B **76**, 085210 (2007).

[17] Y.-C. Wen, G.-W. Chern, K.-H. Lin, J.-J. Yeh, and C.-K. Sun, Phys. Rev. B **84**, 205315 (2011).

[18] R. G. Stearns and G. S. Kino, Appl. Phys. Lett. **47**, 1048–1050 (1985).

[19] H.-P. Chen, Y.-C. Wen, Y.-H. Chen, C.-H. Tsai, K.-L. Lee, P.-K. Wei, J.-K. Sheu, and C.-K. Sun, Appl. Phys. Lett. **97**, 201102 (2010).

[20] C.-L. Hsieh, K.-H. Lin, S.-B. Wu, C.-C. Pan, J.-I. Chyi, and C.-K. Sun, Appl. Phys. Lett. **85**, 4735–4737 (2004).

[21] J. Homola, S. S. Yee, and G. Gauglitz, Sens. Actuators, B **54**, 3 (1999).

[22] P.-A. Mante, Y.-C. Wu, C.-Y. Ho, L.-W. Tu, and C.-K. Sun, Nano Lett. 13, 1139 (2013).

[23] M. Redwood, Mechanical Waveguides (Pergamon Press, New York 1960), p. 135.

Chapter 5

Hypersonic Pulse Transmission between Bulk Substrate and Nanorod Arrays

5.1 Introduction

In the previous chapters, we have successfully excited LSPs in the gold nanodisk array on top of GaN nanorod in order to make each gold nanodisk as an independent opto-acoustic sensor (Chapter 2). Then the interaction between LSPs and CAMs of gold nanodisk was experimentally investigated, which confirmed that the intense LSPs field indeed increased the hypersonic detection sensitivity (Chapter 4). For phased array imaging application, it is critical to apply this structure to passively detect the hypersonic waves and to study the effect of the array periodicity. Fig. 5.1 presents the scheme showing the detection of the propagated hypersonic waves by one gold nanodisk on top of a GaN nanorod, which was connected to a GaN substrate. The propagated hypersonic waves were assumed to be coupled either from a liquid sample or a solid sample through a matching layer into the GaN substrate, then propagated toward the GaN nanorod. After scattered at the interface between the nanorod and the substrate, part of the hypersonic waves would be coupled into the nanorod, and then propagated as the AGM in the nanorod [1, 2]. The hypersonic signal would finally be detected by the gold nanodisk through coupling to its vibrational modes [3, 4]. The vibration of the gold nanodisk will modify the LSP effect and will be eventually detected by an optical probe.
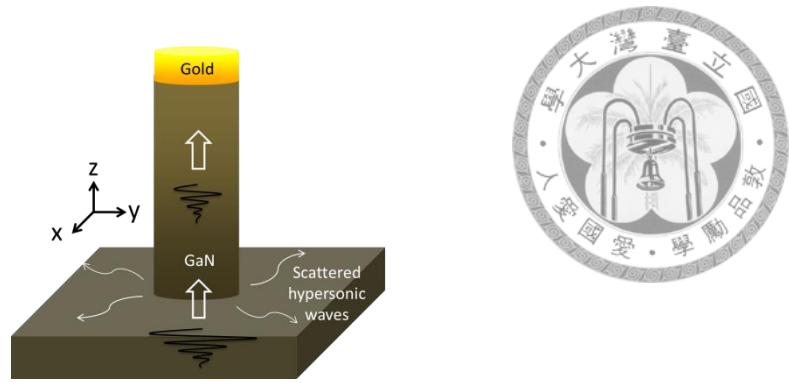
Figure 5.1 Schematic showing the detection of propagated hypersonic waves by one gold nanodisk on top of a GaN nanorod.

5.2 Slowness Curve of GaN

Since hypersonic pulse propagates in the GaN single crystal, we first calculated all possible acoustic modes in wurtzite GaN. Fig. 5.2(a), (c) are the schematic showings of the direction of the propagated acoustic modes and Fig. 5.2(b), (d) show the slowness curves (the reciprocal of sound velocity) for wurtzite GaN as a function of propagation vector for out-of-c-plane and in-c-plane acoustic waves. P (primary) wave is the longitudinal acoustic mode, which has the fast sound velocity. SV (shear vertical) and SH (shear horizontal) waves are the transverse acoustic mode, whose sound velocities are slower than the longitudinal mode. Since GaN is an anisotropic crystal, the sound velocity is dependent of the angle of propagated direction for out-of-c-plane acoustic mode. On the other hand, one can observe that the sound velocities of all acoustic modes propagate on the c-plane are not angle dependent due to the fact that the crystal structure is symmetric on the c-plane. From the slowness curves, the sound velocities of the fast and slowest acoustic mode are 8020 m/s and 4130 m/s, respectively. Based on the discussion in section 3.3, the two lowest detectable frequencies by the 150 nm gold nanodisk are 11 GHz, and 21 GHz. Meanwhile the design of our hypersonic array is
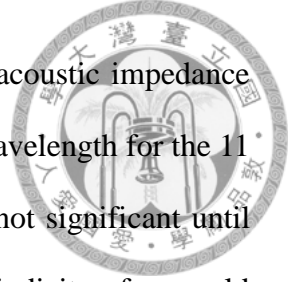
intended to detect the 11 GHz hypersonic waves due to the smaller acoustic impedance mismatch between nanorod and substrate. Therefore the shortest wavelength for the 11 GHz hypersonic waves in GaN is 375 nm. Since grating lobes are not significant until spatial sampling is more than one wavelength [5], therefore the periodicity of our gold nanodisk array is chosen to be slightly shorter than 375 nm in order to accommodate all different modes. Fig. 5.2(e) further compares the dispersion curves of surface acoustic wave (SAW) mode as well as SV, SH, P modes. This result indicates that the scattered hypersonic waves in Fig. 5.1 may propagate with 3932 m/s on the wurtzite GaN surface. In this study, we only focus on the longitudinal mode propagating along the c-axis. In order to study the effect of array periodicity, the periodicities of our arrays are chose as 250 nm, 300 nm, 350 nm and 400 nm. The length of nanorod is set as 120 nm and 220 nm for LSPs excitation [6].
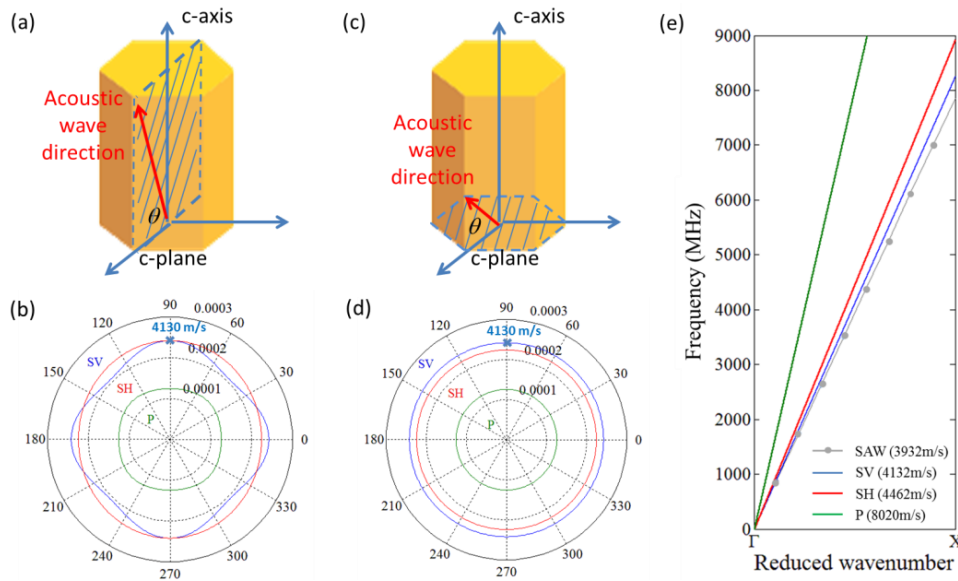
Figure 5.2 Schematic showings of the propagated direction of (a) out-of-c-plane and (c) in-c-plane acoustic mode. Calculated slowness curves in wurtzite GaN for (b) out-of-c-plane and (d) in-c-plane acoustic wave propagation. (e) Dispersion curves of SAW, SV, SH, P acoustic mode in wurtzite GaN.

5.3 Simulated Hypersonic Pulse Transmission at Nanorod/Substrate Interface
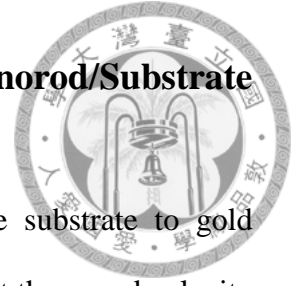
In the simulation, we launched a hypersonic pulse from the substrate to gold nanodisks on top of GaN nanorod with different periodicities. We set the sound velocity in gold and GaN as 3240 m/s and 8020 m/s. Fig. 5.3(a) shows the boundary condition in our simulation, the yellow surface is the free surface (no constraints and no loads acting on the boundary) and hypersonic pulse with 150 nm pulse width [7] is launched from the blue surface below our structure. Pink surface at the bottom of the structure is set as low-reflection boundary condition to simulate the infinite space and transparent surfaces is set as periodic boundary condition so that we can only calculate the unit cell of the array structure. Theoretically the longitudinal pulse will first transfer to the fundamental AGM in the GaN nanorod, and then couple to the CAMs of gold nanodisk. The signal detected by gold nanodisk is obtained by calculating the volume change of gold nanodisk in the lateral direction. Fig. 5.3(b) is the signal detected by single gold nanodisk on top of 120 nm GaN nanorod array with a 250 nm periodicity (simulated by the finite element method, COMSOL Multiphysics, COMSOL, Inc.). Oscillation with 91 ps (11 GHz), which corresponds to the fundamental CAM of 150 nm-diameter gold nanodisk, can clearly be observed. Fig. 5.3(c) is the Fourier Transform of Fig. 5.3(b), which is the frequency spectrum of our detected signal. We can not only observe the fundamental mode (11 GHz), but also the high-order vibrational mode (22 GHz) of 150 nm gold nanodisk. It is noted that we are not able to observe the 18 GHz vibrational mode due to the poor coupling efficiency between fundamental GAM of GaN nanorod and 18 GHz vibrational mode of gold nanodisk, as we discussed in chapter 3.2.

Figure 5.3 (a) The schematic showing the boundary condition in the simulation (yellow: free surface, blue: source surface, pink: low reflecting boundary condit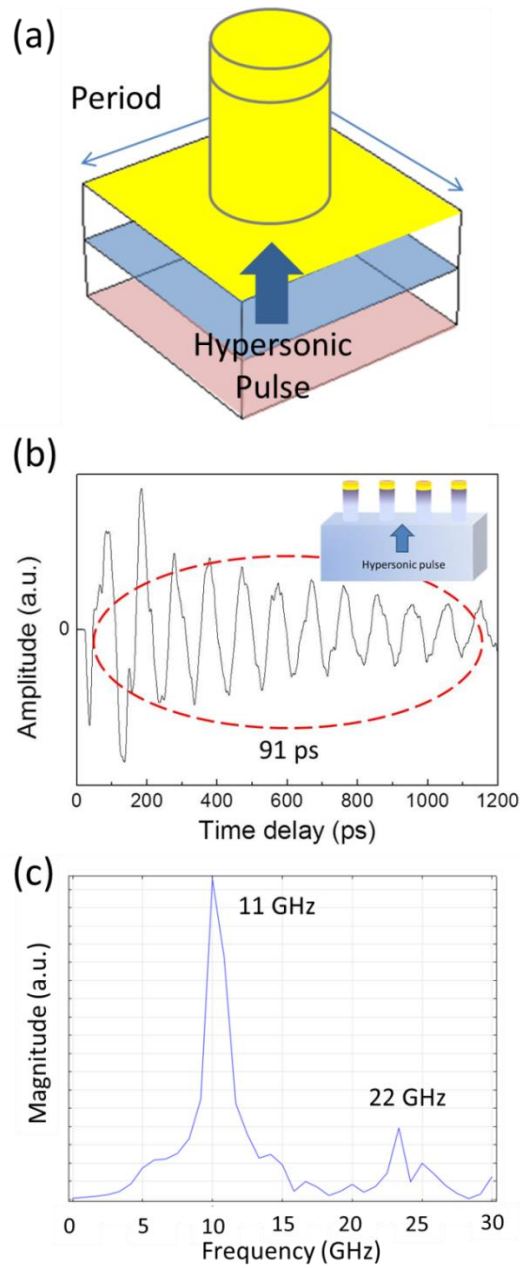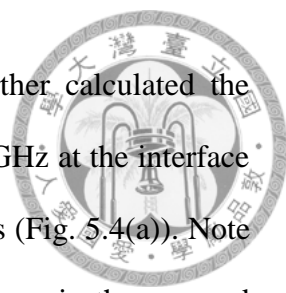ion, transparent: periodic boundary condition). (b) The simulated signal detected by gold nanodisk on top of GaN nanorod arrays, with 150 nm rod diameter, 120 nm rod length and with 250 nm periodicity. (c) Frequency spectrum of the detected signal in Fig. 5.3(b).

In order to study the effect of the array periodicity, we further calculated the transmission coefficient for hypersonic waves with 11 GHz and 22 GHz at the interface between bulk substrate and nanorod array with different periodicities (Fig. 5.4(a)). Note that the transmission coefficient is obtained by comparing the pressure in the nanorod and the initial source pressure. One can first observe that the transmission efficiency for 22 GHz hypersonic waves is lower than 11 GHz case due to the larger acoustic impedance mismatch between nanorod and substrate for 22 GHz hypersonic waves, as we discussed in chapter 3.3. Furthermore the transmission is higher for nanorod arrays with 187 nm and 350 nm periodicities for 22 GHz hypersonic waves. Based on the dispersion curves in Fig. 5.2(e), the sound velocity of SAW mode at the surface of wurtzite GaN is 3932 m/s and the hypersonic wavelength is 179 nm for 22 GHz. This result indicates that although we initially only launch the longitudinal hypersonic pulse, this longitudinal pulse may be scattered into the other surface modes at the interface between the nanorod array and substrate due to the acoustic impedance mismatch. The scattered surface modes could induce resonant transmission when the array periodicity is the integer multiple of their wavelength and lead to enhancement on the detected signal. However such resonant enhancement is not observed when the periodicity of the array is close to the wavelength of 11 GHz hypersonic waves (358 nm). This result may be attributed to the much reduced acoustic impedance mismatch between bulk substrate and nanorod for 11 GHz hypersonic waves. The magnitude of the scattered surface mode is thus not as strong as the 22 GHz case. Meanwhile, one can also observe that the transmission of 11 GHz hypersonic waves reaches its maximum for the array with a 187 nm periodicity. To understand this phenomenon, in Fig. 5.4(b) we simulated the displacement field distribution for 11 GHz hypersonic waves in the GaN nanorod array

53

with a 187 nm periodicity and a 120 nm rod length. As Fig. 5.4(b) shows, the displacement field is mainly located in the nanorod rather than being scattered at the rod/substrate interface. Furthermore this displacement field is very similar to the field of the extensional mode of nanorod [8-10], which suggests that the extensional-vibration-like mode of GaN nanorod may couple to each other for array with a very short periodicity. The frequency of the coupled mode would shift with periodicity. For example, the frequency of the coupled mode shifts from 11.5 GHz to 10.6 GHz by increasing the periodicity of 120 nm GaN nanorod array from 170 nm to 200 nm, as shown in Fig. 5.4(b). When the coupled mode frequency matches the frequency of the incoming hypersonic waves, an enhanced transmission was thus observed. To suppress this coupling effect, which would lead to cross-talk between neighboring pixels in the imaging array application, the most straightforward solution is to change the rod length so as to shift the extensional mode frequency away from the desired detection frequency. By increasing the rod length to 220 nm, our simulation indicated that a similar mode would be excited by 6 GHz hypersonic waves (Fig. 5.4(b)). It also suggested that the detected signal of the fundamental vibrational mode of gold nanodisk on top of the 220 nm-length GaN nanorod is not altered by the array periodicity within our studied range.
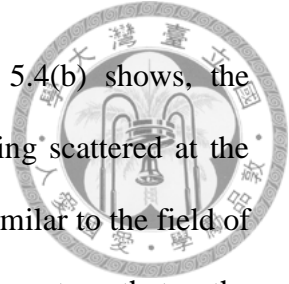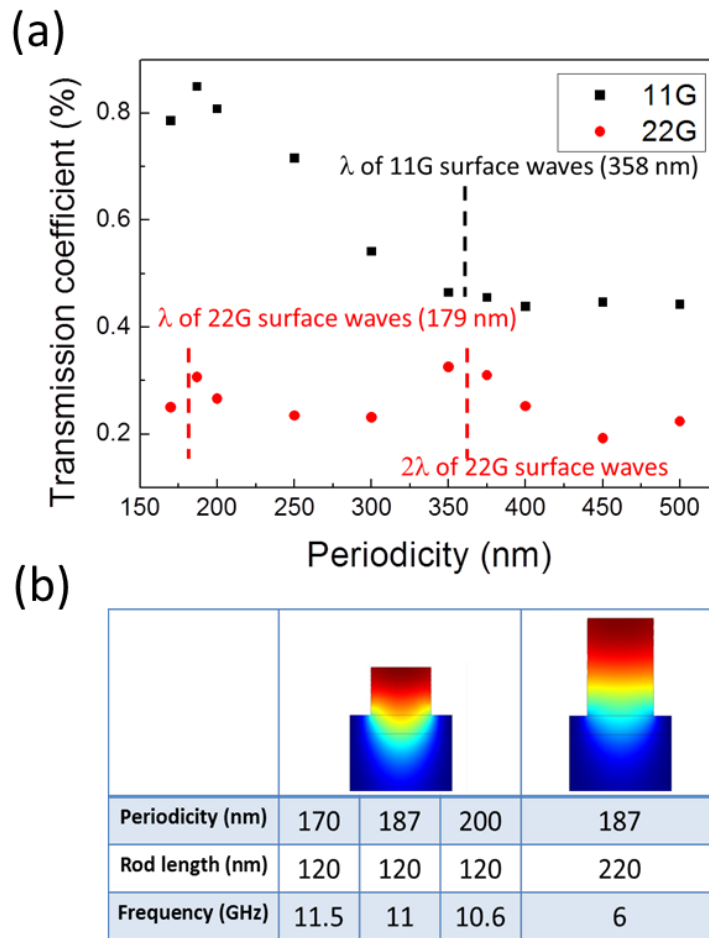
Figure 5.4 (a) Transmission coefficient sat the interface between bulk substrate and GaN nanorod array with different periodicities for hypersonic waves with different frequencies. (b) Displacement field distribution excited by 11.5 GHz,11 GHz, 10.6 GHz and 6 GHz hypersonic waves for the GaN nanorod arrays with 120 nm rod length and 170 nm, 187 nm, 200 nm periodicities as well as 220 nm rod length and 187 nm periodicity.

5.4 Hypersonic Pulse Transmission at Nanorod/Substrate Interface

To study the signal detected by gold nanodisk in our studied sample experimentally and verify our simulated result, we launched hypersonic pulses from the interface between GaN and sapphire substrates by 360 nm femtosecond pump pulses and

detected the gold nanodisk vibration by 720 nm femtosecond probe pulses. The light source of such a transmission-type pump-probe system [11, 12] is a mode-locked Ti:sapphire laser (Coherent Mira 900) with a 100 fs pulse width and a 76 MHz repetition rate with an output wavelength of 720 nm. The output pulses were frequency-doubled to 360 nm by a BBO crystal to serve as our pump pulses, which were used to generate the hypersonic pulses from the GaN substrate through deformation potential coupling [13-15]. With an absorption depth of 75 nm in GaN, the pulse width of the generated longitudinal acoustic pulse was approximately twice the absorption depth of the pump beam, which was 150 nm [7]. The 720 nm probe beam was responsible for the excitation of LSPs and acousto-optical detection. The upper part of Fig. 5.5 compares the measured extinction spectra of gold nanodisk on top of 120 nm GaN nanorod with different periodicities. The maximum of the extinction spectra indicates the resonant wavelength of the excited LSPs, which is independent of the array periodicity. To enhance the detection sensitivity, the wavelength of the probe beam was chosen to be 720 nm, which was near the maximum of the frequency derivative of the extinction spectrum.
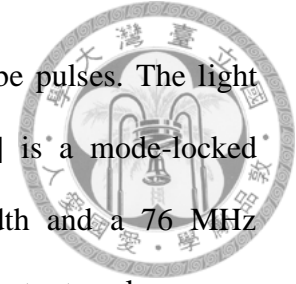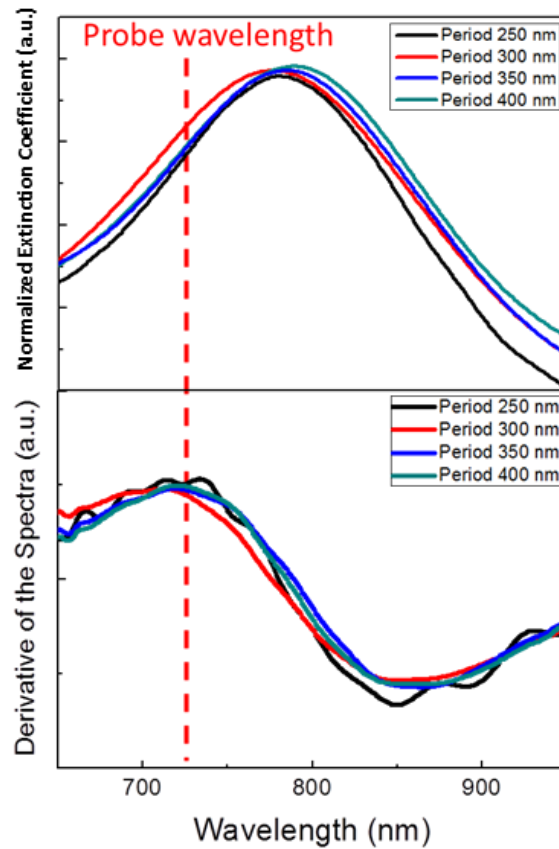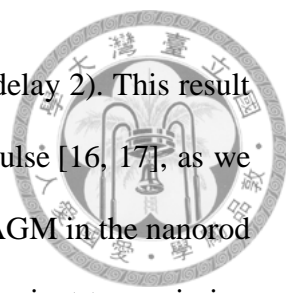
Figure 5.5 Normalized Experimental extinction spectra and the derivative of spectra of the gold nanodisks on 120 nm-length nanorods with different periodicities.

Both pump beam and probe beam were incident from the bottom side of the GaN substrate, as shown in Fig. 5.6(a). The diameters of the pump and probe beams at focus were respectively 20 μm and 30 μm, which are much smaller than the area covered with nanostructures (300 μm × 300 μm). The average power of the pump and probe at the sample surface were 40 mW and 4 mW, respectively. Fig. 5.6(b) is the background removed transient transmission changes of probe beam in our studied sample, while original trace is shown in the inset of Fig. 5.6(b). By observing the background removed transient transmission change, one can see that the transmission change start to increase at

370 ps (time delay 1) and oscillation is observed after 421 ps (time delay 2). This result can be explained by the interaction of plasmons and the hypersonic pulse [16, 17], as we discussed in chapter 4.2. After hypersonic pulse transforms into the AGM in the nanorod and enters the plasmonic field in the nanorod (time delay 1), the transient transmission starts to be modulated due to the fact that the AGM modulates the refractive index of GaN nanorod and modifies the property of LSPs (Fig. 5.6(c)). At time delay 2, the travel distance of hypersonic waves is 3.37 µm, which is very closed to the averaged substrate thickness before etching (3.4 µm), the AGM thus reaches the interface between gold and GaN. Since plasmonic field is well-confined at this interface, the modulation thus reaches its maximum (Fig. 5.6(d)). After hypersonic pulse passed through gold/GaN interface, part of the hypersonic waves will be transferred into the CAMs of gold nanodisk, while the rest of the hypersonic waves will be reflected from the gold/air interface with a π-shift in the phase and generate the opposite signal compared to the first part. Therefore we not only observe another part of the bipolar signal, but also the oscillations contributed from the CAMs of gold nanodisk.
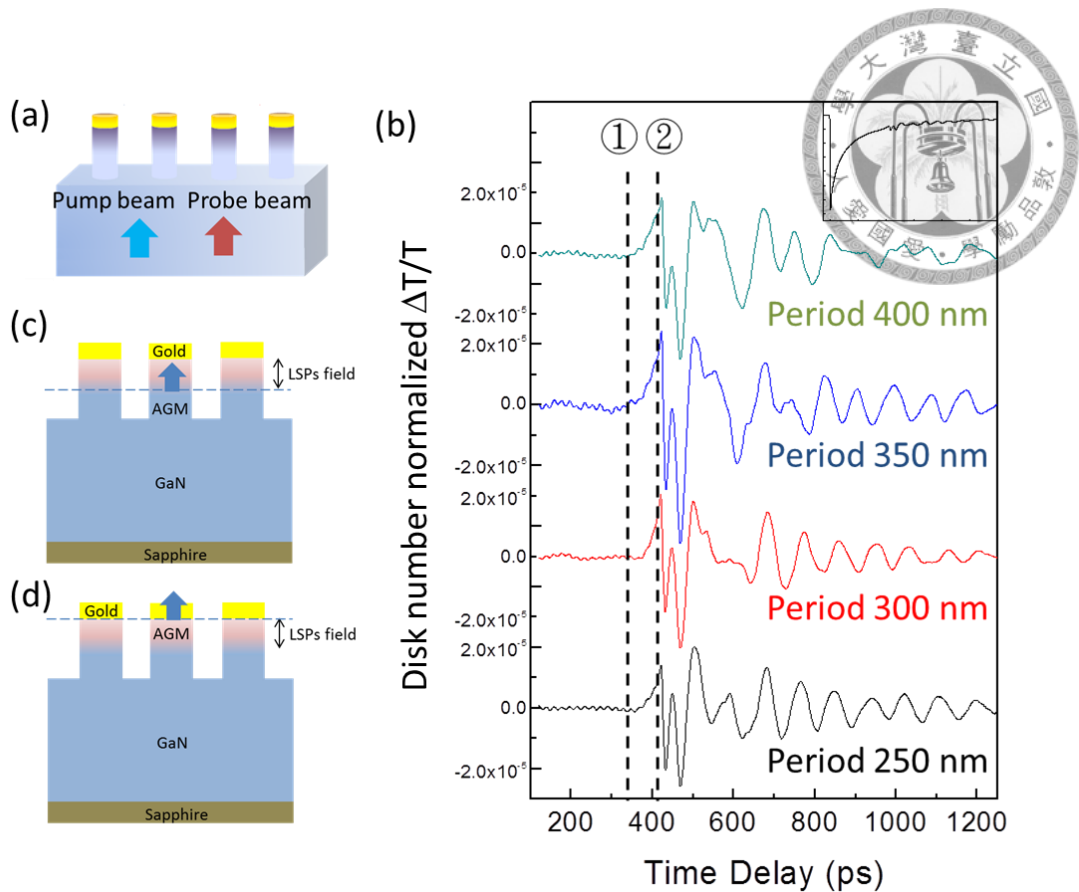
Figure 5.6 (a) The schematic showing of the incident direction of pump beam and probe beam. (b) Background removed transient transmission change for gold nanodisk on top of GaN nanorod array with different periodicities after normalizing the gold nanodisk number for different array periodicity (Inset: the original transient transmission change). (c), (d) Locations of the excited hypersonic pulses at time delay 1 and time delay 2 in Fig. 5.5(b), respectively.

Fig. 5.7 shows the results of time-frequency analysis of the trace in Fig. 5.6(b), which indicates that oscillation is mainly consisted by fundamental (11 GHz) and high-order (22 GHz) vibrational mode. One can also observe that the magnitude of fundamental vibrational mode (11 GHz) is increased by decreasing the periodicity of the array and the magnitude of high-order mode (22 GHz) is only enhanced in the array with

a 350 nm periodicity. The trend of the detected signals for 11 GHz and 22 GHz are in excellent agreement with our simulation (Fig. 5.4(b)). Note that the 18 GHz vibrational mode was also observed in the experiment, but its magnitude was much weaker than the 11 GHz and 22 GHz vibrational modes, as expected from our simulation result due to weak coupling between the fundamental AGM and the 18 GHz vibrational mode. We further compares the 11 GHz signal detected by the gold nanodisks with different periodicities on 120 nm-length and 220 nm-length GaN nanorods. One can see that the 11 GHz signal detected by the gold nanodisks on top of 220 nm nanorods is not dependent of the array periodicity due to the fact that the frequency of coupled extensional-like mode of GaN nanorod is far away from 11 GHz.
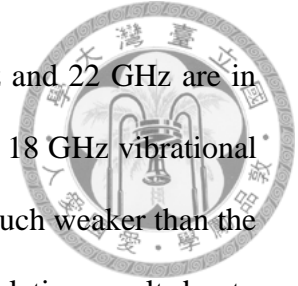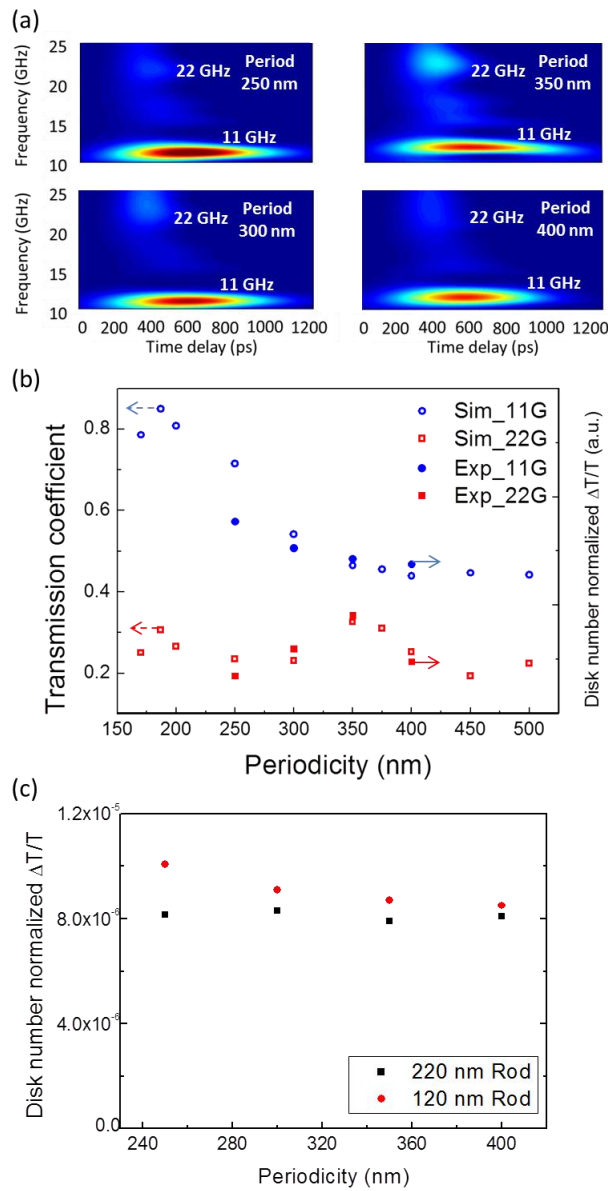
Figure 5.7 (a) Results of time frequency analysis of transient transmission changes for gold nanodisks on top of GaN nanorod arrays with different periodicities. (b) Comparison of the normalized transmission coefficient in the simulation and the normalized transient transmission change in the experiment for 11 GHz and 22 GHz hypersonic signal in arrays with different periodicities (c) Periodicity dependency of the detected 11 GHz signal by gold nanodisks on top of nanorods with 120 nm and 220 nm rod lengths

In this chapter, we demonstrated that hypersonic pulse can be detected by the gold nanodisk array on top of GaN nanorod by coupling it to the CAMs of gold nanodisk. By considering the sound velocity of hypersonic waves in nanorod, our result suggests that the detection frequency of the hypersonic imaging array should be the fundamental vibrational frequency of the nanodisk detector in order to avoid the high acoustic impedance mismatch between nanorods and substrate. Furthermore both the periodicity and the length of nanorod need to be considered in designing future hypersonic array. The periodicity of the array should be smaller than the wavelength of the scattered surface hypersonic waves to avoid the resonance of surface hypersonic waves, which induced the undesired cross talks between pixels. However, the effect of the coupling of the extensional-vibration-like mode of nanorod should be concerned in such close-packed array. To suppress this effect, length of the nanorod should be modified so that the frequency of such coupled mode would be away from the desired detection frequency. So far, we have demonstrated that cross talk between each gold nanodisk can be suppressed both optically and acoustically by exciting LSPs in the nanorod and choosing appropriate array periodicity, respectively. By considering all this phenomena in the array designing, our work basically indicates that gold nanodisks on top of GaN nanorod array have a great potential to be served as an efficient hypersonic array with high detection sensitivity.

Reference

[1] P.-A. Mante, Y.-C. Wu, C.-Y. Ho, L.-W. Tu, and C.-K. Sun, Nano Lett. **13**, 1139 (2013).

[2] S.-C. Yang, Y.-C. Wu, P.-A. Mante, C.-C. Chen, H.-P Chen, H.-Y Chou, M.-H Shih,

and C.-K Sun, Appl. Phys. Lett. **105**, 243101 (2014).

[3] T. R. Gururaja, W. A. Schulze, L. E. Cross, R. E. Newnham, B. A. Auld, and Y. J. Wang, IEEE Trans. Sonics Ultrason. **32**, 481 (1985).

[4] K. C. Cheng, H. L. W. Chan, C. L. Choy, Q. R. Yin, H. S. Luo, and Z. W. Yin, IEEE Trans. Ultrason. Ferroelectr. Freq. Control **50**, 1177 (2003).

[5] C.H. Frazier, IEEE Trans. Ultrason. Ferroelectr. Freq. Control **45**, 196 (1998).

[6] S.-C. Yang, P.-K. Wei, H.-H. Hsiao, P.-A. Mante, Y.-R. Huang, I.-J. Chen, H.-C. Chang, and C.-K. Sun, Appl. Phys. Lett. **105**, 211103 (2014).

[7] S. Wu, P. Geiser, J. Jun, J. Karpinski, and R. Sobolewski, Phys. Rev. B **76**, 085210 (2007).

[8] S. O. Mariager, D. Khakhulin, H. T. Lemke, K. S. Kjaer, L. Guerin, L. Nuccio, C. B. Sørensen, M. M. Nielsen, and R. Feidenhans'l, Nano Lett. **10**, 2461 (2010).

[9] M. Hu, X. Wang, G. V. Hartland, P. Mulvaney, J. P. Juste, and J. E. Sader, J. Am. Chem. Soc. **125**, 14925 (2003).

[10] P.-A. Mante, C.-Y. Ho, L.-W. Tu, and C.-K. Sun, Opt. Express **20**, 18717 (2012).

[11] K.-H. Lin, G.-W. Chern, Y.-C. Huang, S. Keller, S. P. DenBaars, and C.-K. Sun, Appl. Phys. Lett. **83**, 3087 (2003).

[12] P.-A. Mante, H.-Y. Chen, M.-H. Lin, Y.-C. Wen, S. Gwo, and C.-K. Sun, Appl. Phys. Lett. **101**, 101903 (2012).

[13] A. Bartels, T. Dekorsy, H. Kurz, and K. Köhler, Phys. Rev. Lett. **82**, 1044–1047 (1999).

[14] O. B. Wright and V. E. Gusev, Appl. Phys. Lett. **66**, 1190–1192 (1995).

[15] Y.-C. Wen, G.-W. Chern, K.-H. Lin, J.-J. Yeh, and C.-K. Sun, Phys. Rev. B **84**, 205315 (2011).

[16] S.-C. Yang, H.-P. Chen, H.-H. Hsiao, P.-K. Wei, H.-C. Chang, and C.-K. Sun, Opt. Express **20**, 16186 (2012).

[17] H.-P. Chen, Y.-C. Wen, Y.-H. Chen, C.-H. Tsai, K.-L. Lee, P.-K. Wei, J.-K. Sheu, and C.-K. Sun, Appl. Phys. Lett. **97**, 201102 (2010).

.

Chapter 6

Summary and Future Aspect

The main purpose of this thesis is to investigate the possibility of hypersonic imaging array. In the beginning, the plasmonic behavior in different nanostructure is first discussed for increasing the hypersonic detection sensitivity. Our result indicates that gold nanodisks on top of GaN nanorod can efficiently confine the plasmonic field in the high refractive index nanorod, which suppresses the plasmonic coupling and induces the LSPs. Based on this structure, behavior of acoustic phonons in the gold nanodisk and GaN nanorod is then investigated in chapter 3. CAMs of gold nanodisk and the AGM in GaN nanorod were introduced and the coupling efficiency between these two modes was studied.

Based on these understandings, we discussed the interaction between CAMs of gold nanodisk and plasmonic field in chapter 4. These results confirmed that the intense LSPs field in the gold nanodisk on top of GaN nanorod array indeed increased the detection sensitivity by optically exciting the CAMs of gold nanodisk. In chapter 5, a hypersonic pulse is launched from GaN substrate to the sample to study the effect of the array periodicity and rod length. Our results suggested that both the periodicity and the length of nanorod need to be considered in designing future hypersonic array. Meanwhile the detection frequency of hypersonic waves is preferred to be the fundamental vibrational frequency of the nanodisk detector in order to avoid the high acoustic impedance mismatch between nanorods and substrate. The periodicity of the array should be smaller than the wavelength of the scattered surface hypersonic waves to avoid the possible resonant enhancement or enhanced coupling effects, so as to avoid the possible

cross talks between pixels. The length of nanorod should also be concerned so that the frequency of coupled extensional-vibration-like mode would be away from the fundamental vibrational frequency of the detector.
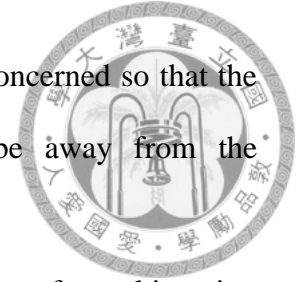
Here we would further propose some ideas to realize such an array for real imaging application. In the traditional acoustic imaging detection setup, most of the measured sample is placed in the water tank. As Fig. 6.1(a) shows, small chip is placed in the water tank to measure the image. Since the slower sound velocity for water (1480 m/s) compared to GaN (8020 m/s), hypersonic waves in water may provide higher spatial resolution owing to smaller wavelength (the wavelength is 5.4 times smaller in water compared to hypersonic waves with the same frequency in GaN). Meanwhile the acoustic impedance matching layer between water and the sapphire substrate should also be developed for hypersonic waves with fundamental vibrational frequency of the nanodisk detector. Except for measuring the sample in the water tank, Fig. 6.1(b) also reveals an idea to measure the sample in the solid (3-D electronic circuit, for example), which can be attached to the hypersonic arrays by wafer bounding. In both systems, signal detected by each nanodisk detector can be probed by scanning near-field optical microscopy. By sampling the detected signal and analyzing the phase, image at different depth below surface can be obtained to construct the 3-D image.
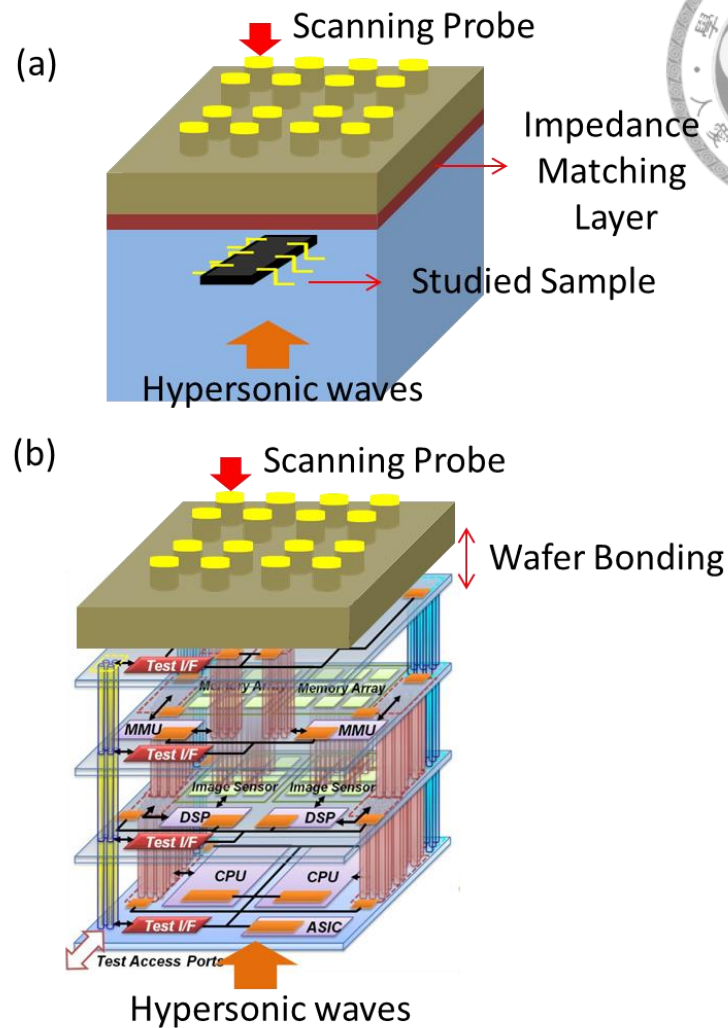
Figure 6.1 Schematic showing the possible detection setups for (a) liquid-based and (b) solid-based hypersonic imaging systems in the future.

In conclusion, we have demonstrated that gold nanodisks array on top of GaN nanorod substrate have a great potential to be served as a hypersonic array with high detection sensitivity. Furthermore by understanding the effect of periodicity and rod length, this work may not only provide an approach to study the transport behavior at the interface between nanostructure and bulk material, but also a guild line for designing future hypersonic imaging system.

Supplementary Materials

Publication List

SCI Journal Publications

1. S.-C. Yang, H.-P. Chen, H.-H. Hsiao, P.-K. Wei, H.-C. Chang and C.-K. Sun, "Near-field dynamic study of the nanoacoustic effect on the extraordinary transmission in gold nanogratings," Opt. Express 20, 16186 (2012).

2. S.-C. Yang, P.-K. Wei, H.-H. Hsiao, P.-A. Mante, Y.-R. Huang, I-J. Chen, H.–C. Chang, and C.-K. Sun, "Enhanced detection sensitivity of higher-order vibrational modes of gold nanodisks on top of a GaN nanorod array through localized surface plasmons," Appl. Phys. Lett. 105, 211103 (2014).

3. S.-C. Yang, Y.-C. Wu, P.-A. Mante, C.-C. Chen, H.-P. Chen, H.-Y. Chou, M.-H. Shih, and C.-K. Sun, "Efficient excitation of guided acoustic waves in semiconductor nanorods through external metallic acoustic transducer," Appl. Phys. Lett. 105, 243101 (2014).

4. P.-A. Mante, C.-C. Chen, Y.-C. Wen, H.-Y. Chen, S.-C. Yang, Y.-R. Huang, I.-J. Chen, Y.-W. Chen, V. Gusev, M.-J. Chen, J.-L. Kuo, J.-K. Sheu, and C.-K. Sun, "Probing Hydrophilic Interface of Solid/Liquid-Water by Nanoultrasonics," Scientific Report 4, 6249 (2014).

5. P.-A. Mante, Y.-R. Huang, S.-C. Yang, T.-M. Liu, A. A. Maznev, J.-K. Sheu, and C.-K. Sun, "THz acoustic phonon spectroscopy and nanoscopy by using piezoelectric semiconductor heterostructures," Ultrasonics 56, 52 (2015).

6. I.-J. Chen, P.-A. Mante, C.-K. Chang, S.-C. Yang, H.-Y. Chen, Y.-R. Huang, L.-C. Chen, K.-H. Chen, V. Gusev, and C.-K. Sun, "Graphene-to-Substrate Energy Transfer

through Out-of-Plane Longitudinal Acoustic Phonons," Nano Lett. 14, 1317-1323 (2014).

7. S.-C. Yang, T.-P. Shen, T.-T. Wu, Y.-R. Huang, and C.-K. Sun, "Investigation of Gold/GaN Nanorod Arrays for Hypersonic Detection: The Effect of Periodicity," submitted to Applied Physics Letters.

8. S.-C. Yang, H.-C. Lin, T.-M. Liu, J.-T. Lu, W.-T. Hung, Y.-R. Huang, Y.-C. Tsai, C.-L. Kao, S.-Y. Chen, and C.-K. Sun, "Efficient Structure Resonance Energy Transfer from Microwaves to Confined Acoustic Vibrations in Viruses," submitted to Scientific Reports.

Conference Publications

1. S.-C. Yang, H.-H. Hsiao, H.-P. Chen, P.-K. Wei, and C.-K. Sun, "Near-Field Interaction between Surface Plasmon Polaritons and Nanoacoustic Waves," in Proceeding of International Photonics Conference, paper C-TH-III1-2, Tainan, Taiwan (Student Paper Award), 2011.

2. S.-C. Yang, H.-H. Hsiao, H.-P. Chen, P.-K. Wei, H.-C. Chang, and C.-K. Sun, "Enhanced near-field interaction between surface Plasmon polaritons and longitudinal nanoacoustic pulses," Abstract Book of 2012 Taiwan-Japan Nanophotonics and Plasmonic Metamaterials Workshop (台日雙邊奈米光電及電漿超穎材料研討會), Taipei, Taiwan (Invited Talk), 2012.

3. S.-C. Yang, H.-H. Hsiao, H.-P. Chen, H.-C. Chang, P.-K. Wei, and C.-K. Sun, "Intense Near-Field Interaction between Surface Plasmon Polaritons and Nanoacoustic Pulses," Conference on Lasers and Electro-Optics, paper QTh3F.8, San Jose, CA, May

2012.

4. S.-C. Yang, H.-H. Hsiao, H.-P. Chen, H.-C. Chang, P.-K. Wei, and C.-K. Sun, "Observation of Near-Field Interaction between Surface Plasmon Polaritons and Nanoacoustic Pulses," 14th International Conference on Phonon Scattering in Condensed Matter, pp. 219-220, Ann Arbor, MI, USA, Jul. 2012.

5. S.-C. Yang, P.-K. Wei, T.-W. Liao, M.-L. Tsai, P.-A. Mante, Y.-R. Huang, I-J. Chen, H.-Y. Chen, and C.-K. Sun, "Strong suppression of angle and period dependency of surface-plasmon-polaritons in gold nanodisks by combining a nanorod substrate," in Technical Digest of Conference on Lasers and Electro-Optics (CLEO2013:Laser Science to Photonic Applications), paper JTu4A.63, San Jose, CA, 2013.

6. S.-C. Yang, P.-K. Wei, H.-H. Hsiao, P.-A. Mante, Y.-R. Huang, I-J. Chen, H.–Y. Chen, and C.-K. Sun, "Strong suppression of angle and period dependency of surface-plasmon-polaritons in a gold nanodisk array by combining a nanorod substrate," in Proceeding of Optics & Photonics Taiwan, International Conference, paper 2013-FRI-S0103-O002, Taoyuan, Taiwan (Best Student Paper Award), 2013.

7. H.-Y. Chen, P.-A. Mante, Y.-R. Huang, S.-C. Yang, I-J. Chen, and C.-K. Sun, "Hypersound Attenuation in Al2O3 Studied by Femtosecond Optical Technique," in Proceeding of Optics & Photonics Taiwan, International Conference, paper 2013-FRI-S0303-O005, Taoyuan, Taiwan, 2013.

8. S.-C. Yang, T.-P. Shen, T.-T. Wu, Y.-R. Huang, and C.-K. Sun, "Investigation of Hypersonic Wave's Transmission at the Interface between a Nanorod Array and a Bulk Substrate," 15th International Conference on Phonon Scattering in Condensed Matter, Nottingham, UK, Jul. 2015.